processes

MDPI

Article

Enhanced Mechanical Properties of Irradiated Ethylene-Vinyl Acetate Copolymer

Anna Svarcova and Petr Svoboda *

Department of Polymer Engineering, Faculty of Technology, Tomas Bata University in Zlin, Vavreckova 5669, 76001 Zlin, Czech Republic; a_svarcova@utb.cz
* Correspondence: svoboda@utb.cz

Abstract: This study investigated the effects of electron beam radiation on the room-temperature and high-temperature mechanical properties of two ethylene-vinyl acetate (EVA) copolymers, designated EVA 206 and EVA 212. These copolymers had varying vinyl acetate (VA) contents (6 wt.% and 12 wt.%), with the same melt flow index of 2.0 g/10 min. Samples were irradiated at doses ranging from 60 to 180 kGy. The impact of electron beam irradiation on the creep, frequency sweep, and stress–strain behaviors of the ethylene-vinyl acetate copolymers was evaluated using a dynamical mechanical analyzer (DMA). Crystallinity was measured using differential scanning calorimetry (DSC) and wide-angle X-ray diffraction (WAXD). Creep compliance was quantitatively analyzed using four-parameter and six-parameter models. While crosslinking had minimal influence on the room-temperature properties, it significantly affected the behavior at 150 °C. With increasing irradiation dose, creep compliance decreased, while the shear modulus, viscosity, and shear stress at a strain of 0.03 increased, indicating enhanced resistance to deformation. Crosslink density also increased with irradiation dose. EVA 212 with a higher vinyl acetate content exhibited a higher resistance to creep and better high-temperature mechanical properties across all measurements.

Keywords: ethylene-vinyl acetate; electron beam irradiation; crosslinking; high-temperature mechanical properties; creep; stress–strain

Academic Editors: George Verros and Raj Kumar Arya

Received: 29 March 2025
Revised: 15 May 2025
Accepted: 16 May 2025
Published: 18 May 2025

Citation: Svarcova, A.; Svoboda, P. Enhanced Mechanical Properties of Irradiated Ethylene-Vinyl Acetate Copolymer. *Processes* **2025**, *13*, 1562. https://doi.org/10.3390/pr13051562

1. Introduction

Ethylene-vinyl acetate (EVA) is a versatile copolymer renowned for its unique combination of properties, bridging the gap between thermoplastics and elastomers [1]. Its inherent flexibility [2], toughness [3], and notable chemical resistance [4] render it suitable for a diverse array of applications across various industries [5]. From footwear [6,7] and adhesives [8] to solar cell encapsulation [9] and medical devices [10], EVA's adaptability stems from the ability to tailor its characteristics by adjusting the vinyl acetate (VA) content during synthesis [11]. This inherent tunability makes EVA a subject of considerable interest for further property modification through advanced processing techniques [12].

One such powerful technique is electron beam irradiation [13], a method that utilizes high-energy electrons to induce significant changes in the structural and chemical makeup of polymeric materials [14]. By precisely controlling the parameters of the electron beam, such as its energy and the delivered dose, it becomes possible to manipulate the properties of polymers like EVA in a targeted manner [2]. This control allows for enhancements like crosslinking [7], which can improve mechanical strength and thermal stability, as well as processes like sterilization, crucial for medical applications [15]. However, alongside these

potential benefits, electron beam irradiation can also induce damage within the polymer structure, leading to undesirable alterations in its performance [16].

Electron beam (EB) irradiation is a common method for crosslinking polymers, leading to improved mechanical properties especially at elevated temperatures. EB irradiation is a valuable tool for tailoring the physical properties of commodity plastics, resulting in enhanced final product characteristics, and has numerous industrial applications [17].

EB irradiation facilitates crosslinking by creating bonds between long polymer chains, resulting in a reinforced molecular structure. This process allows for the controlled and reproducible enhancement in the polymer's physical properties, meeting specific product design requirements. The near-instantaneous nature of the crosslinking reaction enables high production rates (reaching hundreds of meters per minute) with modern high-output EB units, making it a competitive alternative to chemical crosslinking methods.

Electron beam (EB) irradiation processing can significantly improve key polymer properties of polymeric materials, including mechanical properties, thermal stability, chemical resistance, and surface properties. Crucially, crosslinking can enhance creep resistance, a critical property for polymers [17]. Creep, the deformation of a material under constant stress, over time, is a critical consideration for polymers used in applications such as pipes, wires, and storage tanks.

Several studies have investigated EVA blends. Sabet and Soleimani [18] examined the effect of electron beam irradiation on EVA. They studied the impacts of electron beam irradiation on EVA at room temperature, focusing on density, tensile strength, and hardness. Mechanical and thermal properties and volume resistance are dependent on the absorbed dose [18]. Khodkar and Ebrahimi [19] studied the dynamic mechanical properties of EVA across a temperature range below the melting point. The authors observed a decrease in the storage modulus with the increase in the VA content. The storage modulus decreased with increasing VA content and temperature, while it increased with increasing frequency [20]. The findings demonstrated that with an elevation in the VA content within the EVA copolymer, there was a decline observed in both the peak melting temperature and enthalpy. Comparable outcomes have been documented in previous studies by Khonakdar et al. [21], which showed a reduction in EVA crystallinity and melting temperature with higher VA content. Gu and Zhang explored the influence of VA content on the thermal and optical properties of EVA copolymers and further analyzed the suitable application areas of different EVA copolymers [22]. In another work, G. Farias et al. [23] observed that the complex viscosity and storage modulus at low frequencies increased with the increase in the EVA content and followed the mixing rule in blends with polyethylene. The properties of EVA are highly dependent on the VA content, which influences both polarity and elasticity [20,23]. Sethi et al. [24] studied the effect of radiation dose on the dynamic mechanical properties of EVA.

Chattopadhyay et al. [25] found that increasing EVA content in polyethylene blends increased the amorphous characteristic, leading to greater crosslinking efficiency at a specific radiation dose.

Dutta et al. [26] explored the influence of electron beam irradiation on blends of ethylene-vinyl acetate/thermoplastic polyurethane (EVA/TPU), and the results revealed significant improvements in mechanical, thermal, and electrical properties even at low radiation doses. Wang et al. [27] investigated the effects of EVA incorporation into PVC, showing that a higher VA content in EVA led to improved mechanical properties and gel content. Moreover, the gel content of the blends increased proportionally with higher levels of EVA content and active hydrogen atoms within the EVA component.

Unlike previous studies, this research systematically evaluates the high-temperature creep compliance, frequency sweep, and stress–strain relationships of EVA copolymers as a function of irradiation dose and vinyl acetate content. The standard mechanical test is typically performed below the melting point of the crystallites (at 20 °C). At these temperatures, intercrystallite chains form structures with maximum molar mass, and crosslinking occurs between chains connected to different crystallites [28]. The cross-link density at a given irradiation dose depends on the level of amorphous material in EVA. Crystalline regions were only slightly affected by irradiation [18]. The crosslinking takes place in the amorphous region and the surface of the lamellae of the semicrystalline polymer [29]. Testing at temperatures above the melting point eliminates physical crosslinking due to the absence of crystal lamellae. Auhl et al. investigated creep for polypropylene at 180 °C [30].

This paper examines the EB irradiation crosslinking of EVA copolymers, specifically focusing on the influence of VA content (branching density) at room and high temperatures (25, 150 °C) on the creep, frequency sweep, and stress–strain behaviors. The creep data were analyzed by the Burger four-parameter model and six-parameter model.

This study aims to (1) examine the effect of radiation dose on crosslinking and (2) determine the influence of VA content on room- and high-temperature mechanical properties. The experimental methods employed include room- and high-temperature creep testing, high-temperature frequency sweep analysis, and stress–strain analysis using a dynamic mechanical analyzer (DMA).

2. Materials and Methods

2.1. Materials

Two different ethylene vinyl acetate copolymers were used in this study: EVA 206 and EVA 212. The chemical structure of these copolymers is shown in Figure 1.

EVA 206: 6 wt. % of vinylacetate ethylene/vinylacetate molar ratio = 48:1 ESCORENE Ultra FL 00206

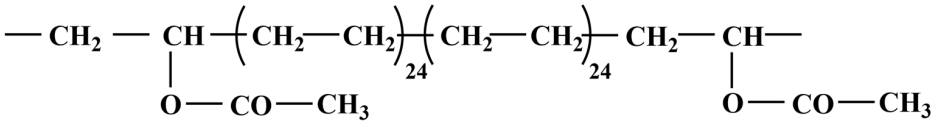

EVA 212: 12 wt. % of vinylacetate ethylene/vinylacetate molar ratio = 23:1 ESCORENE Ultra FL 00212

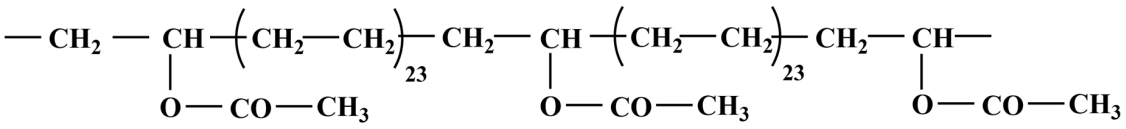

Figure 1. Chemical structure of EVA copolymers.

EVA 206 (trade name Escorene Ultra FL00206, ExxonMobil Chemical, Machelen, Belgium) contains 6 wt.% vinyl acetate and 94 wt.% ethylene, which corresponds to 2.04 mol% vinyl acetate and 97.96 mol% ethylene, with an ethylene/vinyl acetate (ET/VA) molar ratio of 48.10. The density of EVA 206 is 0.926 g/cm^3. Its melting point is 102 °C.

EVA 212 (trade name Escorene Ultra FL00212, ExxonMobil Chemical, Machelen, Belgium) contains 12 wt.% vinyl acetate and 88 wt.% ethylene, which corresponds to

4.26 mol% vinyl acetate and 95.74 mol% ethylene, with an ET/VA molar ratio of 22.50. The density of EVA-212 is 0.934 g/cm^3. Its melting point is 96 °C.

The melt flow index (MFI) at 190 °C was 2.0 g/10 min for all samples.

2.2. Compression Molding

Compression molding was employed according to ASTM D4703 to fabricate 1.0 mm thick sheets using a 12 cm × 6 cm stainless steel frame. The EVA pellets were initially pre-heated at 150 °C under minimal pressure for 5 min, and then the materials were compressed at 10 MPa for 3 min in a hydraulic press and then rapidly cooled in a separate cold press under pressure. Finally, the sheets were rapidly cooled under pressure, achieving an average cooling rate of 25 °C/min.

2.3. Electron Beam Irradiation

Electron beam irradiation was performed at BGS Beta-Gamma-Service GmbH, Wiehl, Germany, at room temperature (25 °C) in air. The source of radiation was the toroid electron accelerator Rhodotron (10 MeV, 200 kW). Samples were conveyed through an irradiation tunnel at a constant speed, receiving doses from 60 to 180 kGy in 30 kGy steps per pass to maintain the sample temperature below 50 °C. Samples were arranged in one layer sealed between PET sheets during irradiation. Other important parameters were 10 mA, a conveyer belt speed of 3 m/min, a scanner-to-sample distance of 78 cm, and an irradiation time of 2 s.

2.4. Room-Temperature and High-Temperature Mechanical Tests

Two tests were performed in the dynamic mechanical analyzer DMA-1 STARe System METTLER TOLEDO Switzerland machine (Mettler-Toledo (Switzerland) GmbH, Greifensee, Switzerland) to determine the material's creep, frequency sweep (0.1–100 Hz), and stress–strain behaviors. Tests were carried out at 25 °C and 150 °C using shear deformation on two samples with a size of 11 mm × 11 mm × 1 mm. Conditions for the creep test in static mode were 1 min at 0.05 N, 5 min at 1.00 N (creep), and 5 min at 0.05 N (recovery). Stress–strain tests utilized a 0–2 N force range with a 0.4 N/min rate, and shear stress was assessed at a shear strain of 0.03. Figures 2 and 3 show shear mode testing in the dynamic mechanical analyzer, METTLER TOLEDO, Greifensee, Switzerland. After the testing, the results of three measurements were always averaged. These measurements are very sensitive to the crosslinking level performed by various methods listed in Appendix A.

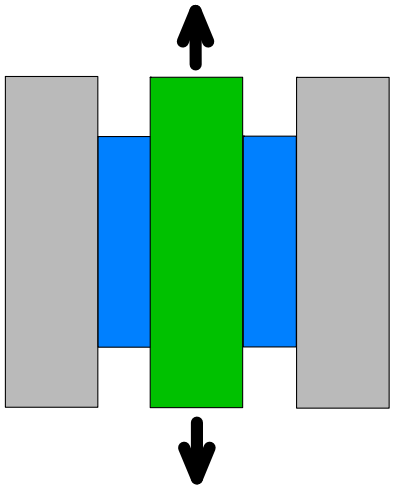

Figure 2. The shear test configuration in the dynamic mechanical analyzer. Two samples (blue rectangles) are sheared between static metal plates (gray rectangles) and a moving central component (green rectangle). The black arrow indicates the movement of the central component, which is used to measure the material's response in μm.

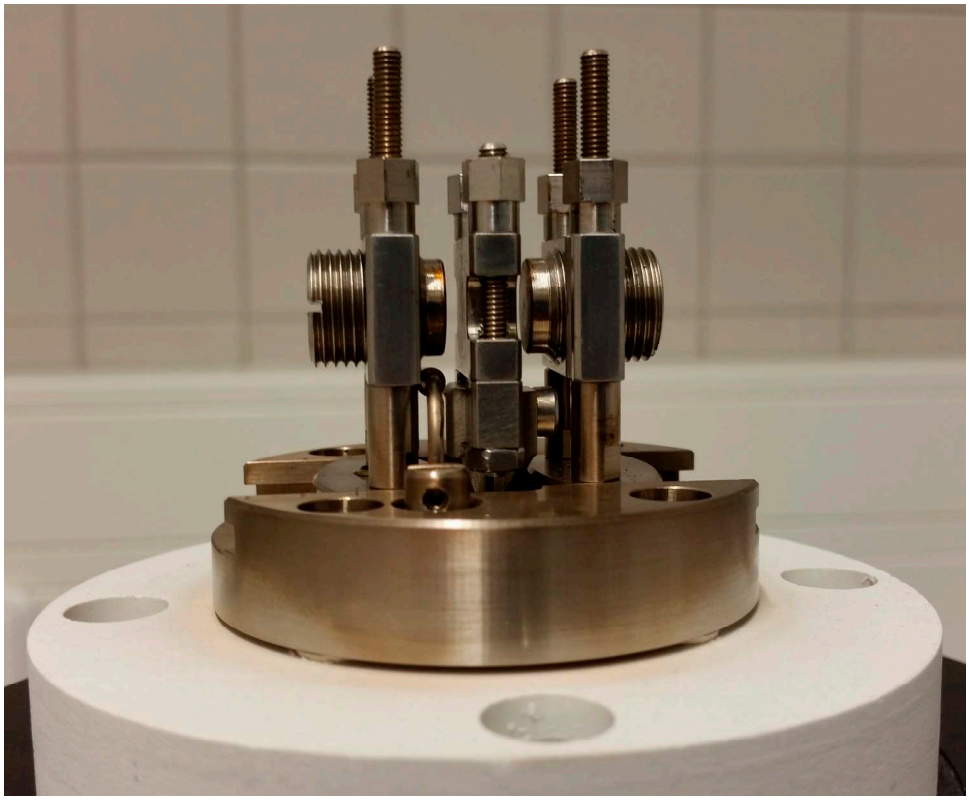

Figure 3. Shear testing fixture of dynamic mechanical analyzer.

Polymers exhibit viscoelasticity, a combination of viscous liquid and elastic solid properties enabling energy dissipation under stress, often assessed by creep tests and influenced by factors like crosslinking and molecular weight. This behavior arises from the interaction of elasticity, described by Hooke's Law $\sigma = E \cdot \varepsilon$, establishing a direct proportionality between stress σ and strain ε through the elastic modulus E. In addition, viscosity, defined by Newton's law of viscosity of $\sigma = \eta \frac{d\varepsilon}{dt}$, is represented by η. The basic Maxwell model, a series spring and dashpot, illustrates immediate elastic strain followed by continuous viscous flow and stress relaxation, while the Kelvin–Voigt model, a parallel arrangement, depicts time-dependent creep and recovery behaviors. More complex models, such as the four-parameter Burgers model (combining Maxwell and Kelvin–Voigt elements in series) and more elaborate six-parameter models (involving further combinations), offer more accurate descriptions by capturing phenomena like permanent deformation and multiple relaxation times. Notably, the statistical correlation between the model's predictions and experimental data, often represented by the R-squared value, typically increases with a higher number of elements incorporated into the viscoelastic model. These refined models provide a deeper understanding of the complex viscoelastic nature of polymers and the impact of their structure on mechanical response [16,31,32].

Figure 4 illustrates the four-parameter model, and creep behavior is described by Equation (1). This model, also known as the Burgers model, represents creep as a combination of mechanical springs and dashpots. Four- and six-element Kelvin–Voight models (also known as Burger models) were fitted to the experimental creep data [33]. The four-element Burgers model, commonly used to simulate the creep behavior of natural fiber-reinforced polymer composites, consists of a Maxwell unit and a Kelvin unit in series [34].

As depicted in Figure 4, the four-parameter Burger model consists of two springs with instantaneous shear compliance J_0 and retarded compliance J_1 and two dashpots with viscosities η_0 and η_1. The mathematical expression for this model is given in Equation (1) [35]. The six-parameter model comprises a Maxwell element (spring and dashpot in series) in series with two Kelvin elements (spring and dashpot in parallel) (Figure 5) [33,36].

Stress relaxation and creep recovery are widely used to study the time-dependent viscoelastic behavior of materials. Both tests explore time-dependent rheology within the linear viscoelastic range and employ mechanical models such as the Kelvin–Voigt model for creep behavior. Creep tests are particularly useful for material characterization and are the preferred method for determining zero-shear viscosity [33].

A four-element Burger's model (Figure 4) can be used for fitting the creep data of the EVA copolymer at 150 °C.

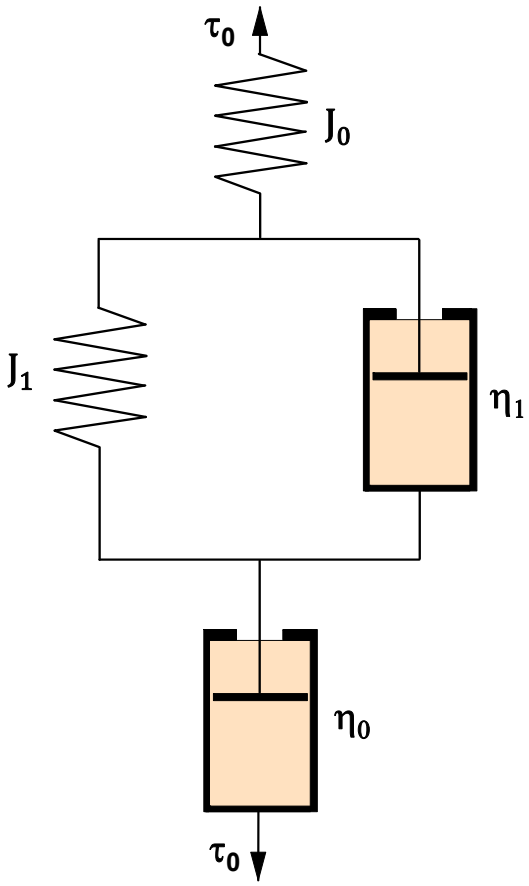

Figure 4. Four-element model for shear creep compliance (Burger model).

$$J(t) = J_0 + J_1\left(1 - e^{-\frac{t}{\lambda_1}}\right) + \frac{1}{\eta_0} \cdot t \quad (1)$$

where

- τ_0 is the applied shear stress, Pa;
- J_0 is the instantaneous shear compliance, Pa^{-1};
- J_1 is the slowed compliance, Pa^{-1};
- η_0 is the zero-shear or Newtonian viscosity, Pa·s;
- λ_1 is the slowing time of slowed element $\lambda_1 = \frac{\eta_1}{G_1}$, s;
- η_1 is the shear viscosity in the viscoelastic region, Pa·s;
- G_1 is the viscoelastic modulus of the slowed element, Pa.

Figure 5 illustrates the six-parameter model. The model is mathematically expressed by Equation (2).

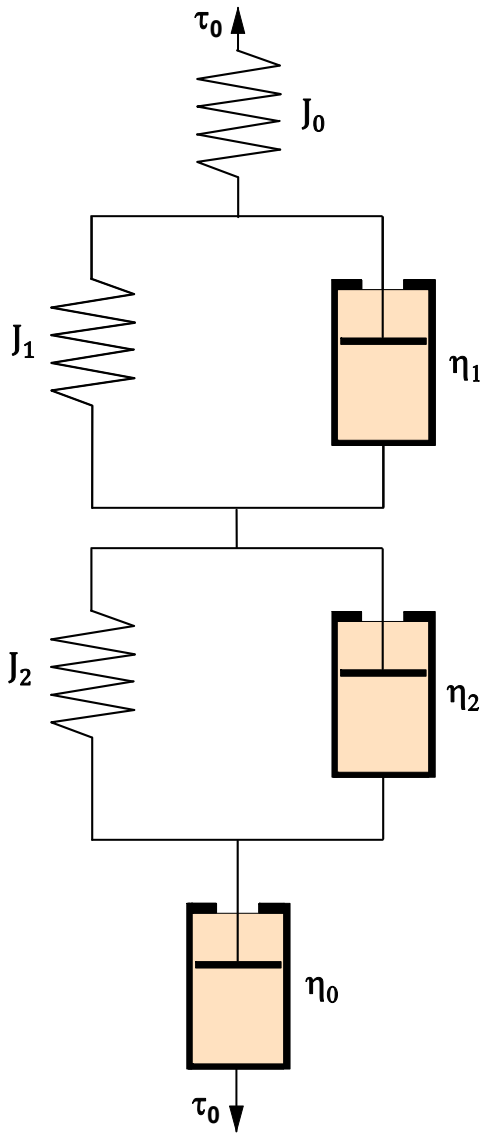

Figure 5. Six-element model for shear creep compliance.

A more precise model of creep behavior contains six parameters and is listed in Equation (2) [37].

$$J(t) = J_0 + J_1\left(1 - e^{-\frac{t}{\lambda_1}}\right) + J_2\left(1 - e^{-\frac{t}{\lambda_2}}\right) + \frac{1}{\eta_0} \cdot t \quad (2)$$

where

- τ_0 is the applied shear stress, Pa;
- J_0 is the instantaneous shear compliance, Pa^{-1};
- J_1 and J_2 are the slowed compliances, Pa^{-1};
- η_0 is the zero-shear or Newtonian viscosity, Pa·s;
- λ_1 and λ_2 are the slowing times of slowed elements $\lambda_1 = \frac{\eta_1}{G_1}$, $\lambda_2 = \frac{\eta_2}{G_2}$, s;
- η_1 and η_2 are the shear viscosities in the viscoelastic region, Pa·s;
- G_1 and G_2 are the viscoelastic moduli of the slowed element, Pa.

- Appendix B explains in detail the coefficient of determination, mathematical sequence of evaluation of creep parameters and the explanation of calculation of molar ratio of vinyl acetate in EVA.

2.5. Frequency Sweep

The relationship between complex viscosity η^* and frequency f in the frequency sweep data is described by a power law:

$$|\eta^*| = kf^n \tag{3}$$

where k and n are material-specific parameters. k is a pre-exponential factor and n is the shear thinning exponent [38].

The parameters k and n can be determined from the logarithmic plot of complex viscosity versus frequency [38]:

$$log|\eta^*| = log\, k + n\, log\, f \tag{4}$$

According to Mussatti and Macosko [39], G^* can be used for the calculation of crosslink density, which is shown in Equation (5).

This equation assumes a rubber-like behavior, where the storage modulus is dependent on temperature and crosslinking density. The value X (crosslinking density) will result in a higher G^* [39].

$$X = \frac{G^*}{R \cdot T} \tag{5}$$

where

- G^* is the complex modulus in Pa;
- X is the crosslinking density (mol/m^3);
- R is the gas constant 8.314 J K^{-1} mol^{-1};
- T is the absolute temperature (in our case 423.15 K).

2.6. Differential Scanning Calorimetry (DSC)

Analysis of the crystallinity was carried out using a differential scanning calorimeter (DSC1) from Mettler Toledo (Columbus, OH, USA). For each measurement, approximately 10 mg of sample was sealed in an aluminum pan, and an empty pan served as the reference. An inert nitrogen environment with a gas flow of 200 mL/min was maintained throughout the experiments. The crystallinity from DSC was calculated by METTLER STARe software (version 18.00b) as a ratio of the heat of fusion of the measured sample over the heat of fusion for the 100% crystalline polymer multiplied by 100. The value of 293 J/g was taken from [40]. Three samples were always measured, and the average values with standard deviations are reported.

2.7. Wide-Angle X-Ray Diffraction (WAXD)

Crystallinity information was acquired through wide-angle X-ray diffraction (WAXD). Diffraction patterns were collected on an XRDynamic 500 diffractometer from Anton Paar (Graz, Austria), operating with Bragg–Brentano geometry in reflection. Copper Kα radiation (λ = 0.154 nm), filtered by nickel, was used as the X-ray source, and the diffraction angle (2θ) was scanned from 10 to 30°. The crystallinity from WAXD was determined by software supplied by Anton Paar called XRDanalysis version 1.2.0.3511 as a ratio of the integral intensities diffracted by a crystalline part and the total integral intensities multiplied by 100. Three samples were always measured, and average values with standard deviations are reported.

3. Results and Discussion

3.1. Polymer Properties

Table 1 lists the properties of the two used EVA copolymers.

Table 1. Properties of ethylene-vinyl acetate copolymers. VA is vinyl acetate, M_n is the number average molecular weight, T_m is the melting point, and MFI is the melt flow index.

Material	VA	VA	M_n	Density	T_m	Crystallinity	MFI
	wt.%	mol%	g/mol	g/cm^3	°C	%	g/10 min
EVA-206	6	2.04	39,000	0.926	102	43.7	2.0
EVA-212	12	4.26	34,000	0.934	96	35.6	2.0

3.2. Crosslink Density Evaluation

The crosslink density was calculated from DMA data at 150 °C. Above the crystal melting point, the absence of crystalline structures permits a more accurate evaluation of crosslinking and entanglement density. In this molten state, the material transitions to a fully amorphous phase.

Figure 6a shows the complex shear modulus G^*, which increases linearly with dose, and its values are higher for EVA 212.

Figure 6b shows crosslink density X at a frequency of 0.1 Hz calculated according to Equation (5). It grows linearly with irradiation. The calculated values of crosslink density are higher for EVA 212.

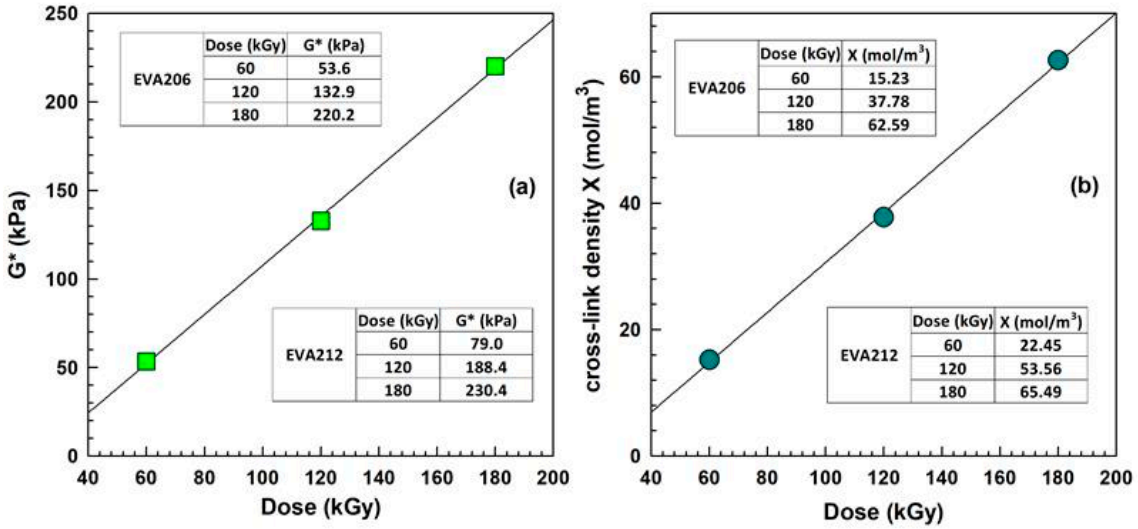

Figure 6. (**a**) Complex shear modulus G^* and (**b**) crosslink density X for copolymer EVA 206 at frequency of 0.1 Hz.

3.3. Room-Temperature Creep Compliance

Figure 7 displays creep compliance curves at room temperature. Notably, EVA 212 exhibits higher creep compliance values. This can be attributed to its higher amorphous phase content, making the material softer and more prone to deformation under stress. A surprising finding is the increased creep for higher irradiation levels, a trend opposite to that observed at 150 °C (see Figures 8 and 9).

This phenomenon is likely due to the coexistence of a physical network alongside the chemical network. While tests at 150 °C primarily detect the chemical network, at 25 °C, a much stronger physical network formed by crystal lamellae plays a dominant role. These

crystal lamellae effectively hold the amorphous chains together during stretching. However, electron beam irradiation appears to cause damage to these crystal lamellae, as evidenced by decreased crystallinity measured using differential scanning calorimetry (DSC) and wide-angle X-ray diffraction (WAXD). For instance, WAXD analysis of EVA 206 showed crystallinity values of 42.03 ± 0.65%, 40.71 ± 0.58%, and 38.42 ± 0.48% for irradiation doses of 60, 120, and 180 kGy, respectively. Similarly, DSC measurements yielded crystallinity values of 42.04 ± 0.73%, 38.64 ± 0.46%, and 36.82 ± 0.67% for the same doses.

Electron beam irradiation of EVA can induce both crosslinking and chain scission, thereby affecting its molecular weight. In pristine semicrystalline EVA, higher-molecular-weight chains form more entanglements, acting as physical crosslinks that resist creep [41]. Additionally, long-molecular-weight amorphous chains serve as tie molecules, crucial for stress transfer between crystalline lamellae and enhancing creep resistance. However, e-beam-induced chain scission reduces the average molecular weight, leading to fewer entanglements and a decrease in the number and effectiveness of tie molecules. This results in weakened interlamellar connections and an increased mobility of shorter chains, ultimately making the EVA more susceptible to creep and increasing its creep compliance.

Consequently, while irradiated EVA demonstrates improved creep resistance at elevated temperatures, it exhibits higher creep values at room temperature. When selecting between irradiated and virgin material, a material engineer must consider both aspects: the enhancement in creep resistance at higher temperatures and the reduction in creep resistance at lower temperatures.

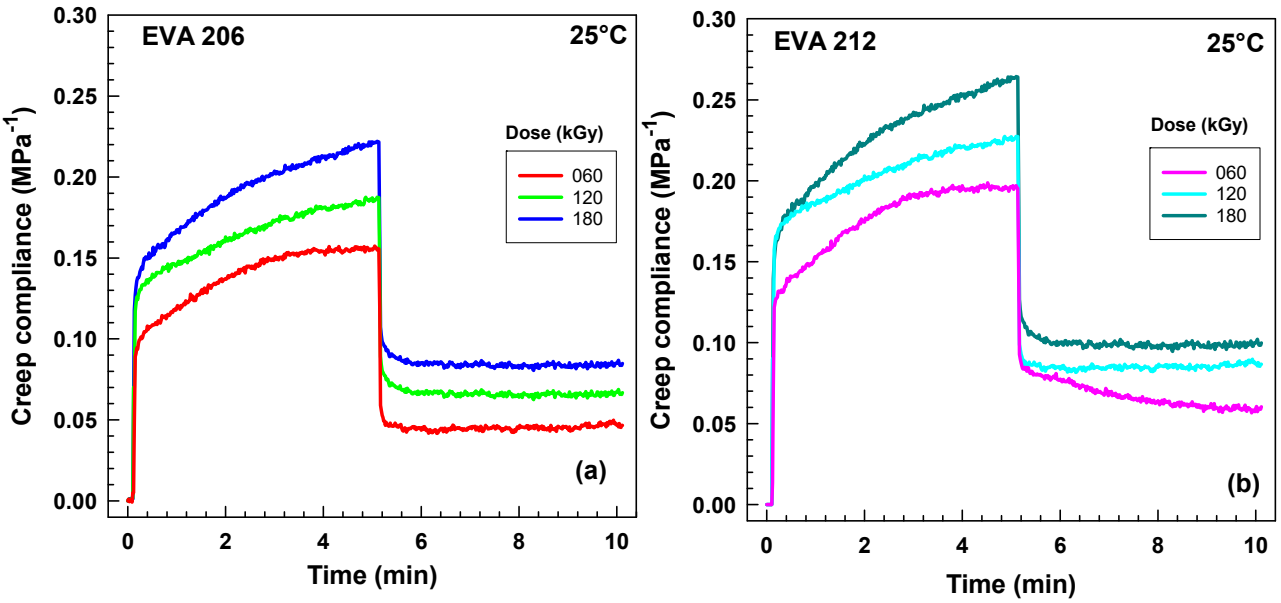

Figure 7. The room-temperature creep compliance during the 5 min creep and 5 min relaxation experiment in DMA (in shear mode) for three irradiation levels (60, 120, 180 kGy): (**a**) EVA 206, (**b**) EVA 212.

3.4. High-Temperature Creep Compliance

Figure 8 shows the creep compliance of EVA 212 as a function of time for three radiation levels (60, 120, 180 kGy). The highest creep was detected for the lowest irradiation (60 kGy). With increasing radiation level, creep compliance gradually decreases. This result implies effective crosslinking. These results are consistent with the findings of Dutta et al. who observed a significant decrease in creep of EVA/TPU blends after crosslinking by electron beam radiation [42]. Auhl et al. observed the same trend for a higher radiation level of long-chain branched polypropylene by electron beam irradiation [30].

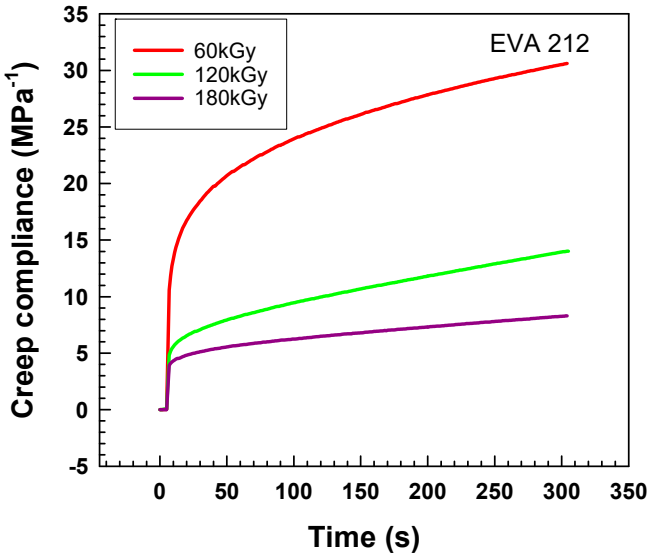

Figure 8. Creep compliance of EVA 212 as a function of time for three radiation levels (60, 120, 180 kGy) at 150°C in shear mode.

Figure 9 illustrates creep compliance curves for EVA 206 and EVA 212, both irradiated at a level of 180 kGy. The instantaneous creep compliance J_0, represented by a spring element in the model, was approximately 4.9 MPa^{-1} for EVA 206 and about 3.9 MPa^{-1} for EVA 212. The subsequent creep behavior is described by a fully reversible viscoelastic Kelvin model (a parallel arrangement of a spring and a dashpot) and an irreversible viscous flow represented by a separate dashpot. After a period of 5 min, the total creep compliance values reached 12.1 MPa^{-1} for EVA 206 and 8.3 MPa^{-1} for EVA 212.

Both the instantaneous creep compliance and the creep compliance after five minutes are lower for EVA 212. This finding indicates a higher degree of crosslinking in EVA 212 compared to EVA 206 under these conditions. This result for EVA aligns well with our previous findings for ethylene-octene copolymers (with 17, 30, and 38 wt.% octene contents) [43], where ethylene copolymers with a higher comonomer content exhibited lower creep compliance after a specific time. This can be attributed to the increased amount of the amorphous phase in those copolymers [17].

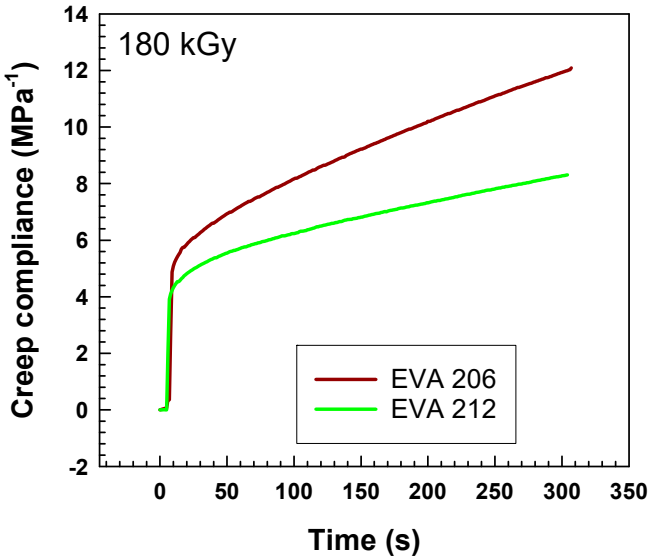

Figure 9. The creep compliance of EVA 206 and EVA 212 as a function of time after irradiation with 180 kGy at 150 °C in shear mode.

When we read the values of creep compliance after 5 min shown in Figure 10, we can plot them as a function of dose. As illustrated in Figure 10, irradiation causes an exponential decay of these values with increasing irradiation. All the values are lower for EVA 212, indicating higher crosslinking.

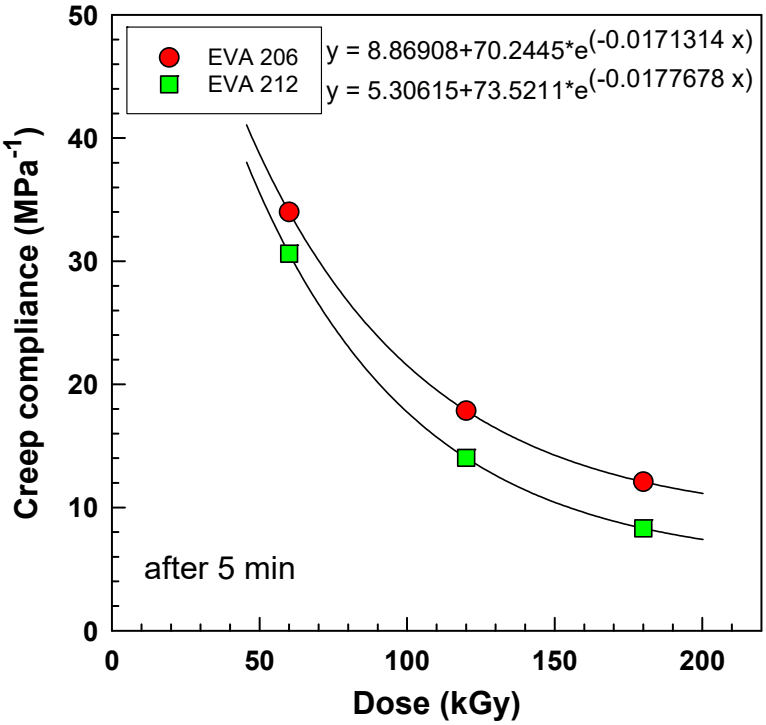

Figure 10. The creep compliance after 5 min at 150 °C as a function of dose fitted by exponential decay functions.

The creep data were analyzed with the help of four- and six-parameter models. Initially, we tested the creep at room temperature, but the results were not conclusive.

In semicrystalline polymers, such as EVA, the crystalline lamellae constrain the amorphous chains at room temperature, and the crosslinking to lower levels is not easily detected. Therefore, our experiments were also carried out at an elevated temperature (150 °C) above the melting point of EVA. At elevated temperature, there are no crystal lamellae and the material is held together only by crosslinking. Shear creep testing was selected over tensile creep due to the expectation of lower crosslink densities, as shear deformation provided more sensitive measurements in this context.

Various mechanical models used to describe system deformation in such tests vary from basic approaches like springs or dashpots to more comprehensive ones involving numerous components [44]. In this study, the viscoelastic behavior of the copolymers was characterized by fitting the creep compliance $J(t)$ values, obtained over a 300 s interval (0 < t < 300 s) and presented in Figure 11, to both four-parameter (Equation (1)) and six-parameter (Equation (2)) models.

The model consists of springs with creep compliance $J(t)$ as elastic elements and of dashpots with viscosity η as a viscous element.

J_0 represents the instantaneous shear compliance of the spring and η_0 describes the viscosity of the dashpot of the Maxwell model. J_1 represents the slowed compliance of a spring and η_1 describes the slowed compliance of a dashpot for the Kelvin–Voight model.

The experimental results from the creep and recovery tests, explained by the four-parameter model, are shown in Figure 11. The creep starts with instantaneous elastic deformation, represented by a spring with shear compliance J_0. This is followed by

slower viscoelastic behavior, described by a Kelvin model with a spring (elasticity) and dashpot (viscosity). The final part of the curve shows viscous flow, leading to irreversible deformation. After five minutes, the stress was released, and the specimen attempted to move back to the original shape. The initial recovery was fast, described by the elastic spring model, followed by slower viscoelastic movement. The viscous flow caused permanent deformation, so the sample could not fully return to its original shape. This creep and recovery curve represents EVA 206-120 kGy.

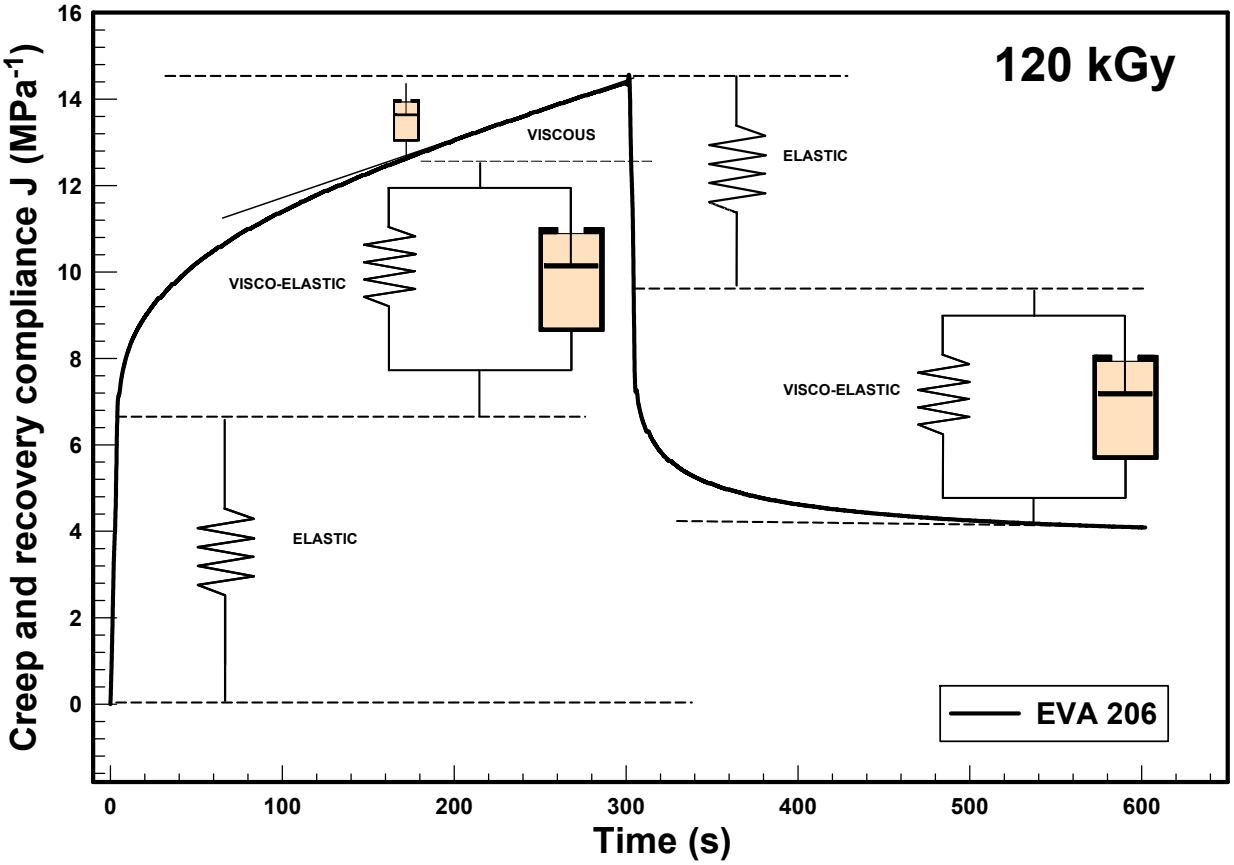

Figure 11. The creep compliance and recovery curve for experimental data of EVA 206-120 kGy with elastic, viscoelastic, and viscous parts of the curve.

Figure 12 shows creep development over time. The curve was fitted with four- (Figure 12a) and six-parameter (Figure 12b) models for a more detailed description of viscoelastic behavior. Creep compliance data (represented by open circles) and the fitted curves (solid-colored lines) are shown for the EVA copolymer at 150 °C. The applied shear stress was 5 kPa (within the linear viscoelastic limit). The fitted curve used a four-parameter Burger's model and six-parameter model.

The six-parameter curve visibly fits the experimental data better. This is because the curve for the six-parameter model passes through the first data point and more accurately follows the overall shape of the experimental points. In contrast, the four-parameter model curve ignores the first data point and does not pass through the center of the experimental points. By designing the experiments and providing the corresponding data for the response variables from the "lack-of-fit" test, the coefficient of determination (R-squared or R^2) was calculated for both models. The R^2 values, presented in Tables 2–5 confirm the visual observations. For instance, the six-parameter model applied to EVA 212 irradiated at 60 kGy (Table 5) yielded an R^2 value of 0.9997, indicating an excellent fit.

In contrast, the four-parameter model (Table 3) resulted in a lower R^2 value (e.g., 0.9972), suggesting a less accurate representation of the experimental data.

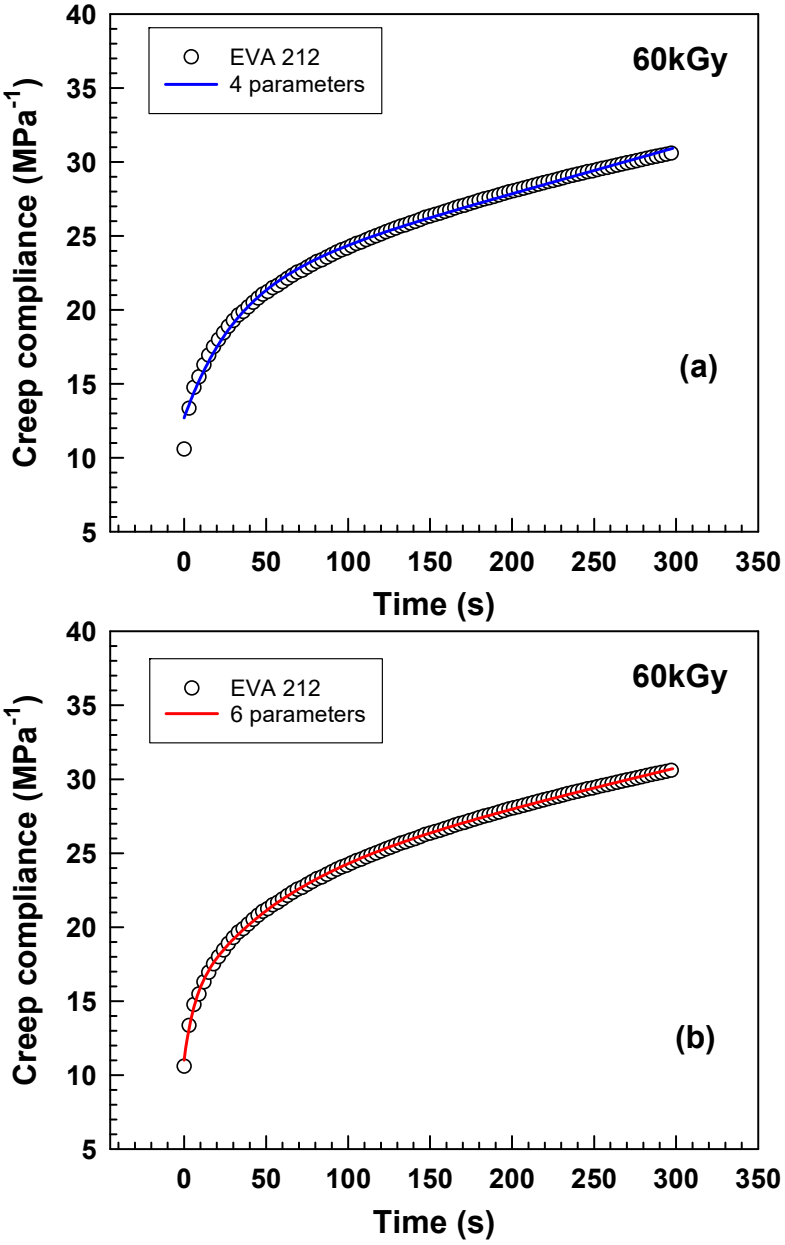

Figure 12. Creep compliance curves of EVA 212 measured by DMA. Experimental data vs. (**a**) four-parameter model with R^2 = 0.9972 and (**b**) six-parameter model with R^2 = 0.9997.

At 180 kGy, the zero-shear viscosity η_0 of EVA 212 is much higher than that of EVA 206 (100.2 Pa·s vs. 53.9 Pa·s, as shown in Tables 2 and 3, respectively). This increase in viscosity with radiation dose is attributed to the increase in molar mass due to crosslinking (a characteristic rheological response of polymeric systems). The developing crosslink network restricts polymer flow at elevated temperatures.

For both EVA copolymers, the creep compliance parameters J_0, J_1, and J_2 decrease with increasing radiation dose. In the four-parameter model, the slowing time λ_1 exhibits a linear decrease with radiation dose. Similarly, in the six-parameter model, λ_2 decreases linearly with radiation dose. However, λ_1 in the six-parameter model shows an increase with radiation dose. The viscosity parameters η_0, η_1, and η_2 and shear moduli G_0, G_1, and G_2 presented in Tables 2–7 consistently increase with radiation dose across all samples.

Table 2. Parameters from the creep analysis of EVA 206 by the four-parameter model. Embedded trends were created in Excel with the Sparkline function. Sparklines are mini-charts placed in a single cell representing a selected column of data.

EVA 206				
Dose (kGy)	J_0 $\left(\mathrm{Pa}^{-1}\right)$	J_1 $\left(\mathrm{Pa}^{-1}\right)$	λ_1 (s)	η_0 (Pa·s)
60	13.00	15.38	40.54	16.68
120	7.44	2.68	38.19	28.16
180	5.21	1.39	36.68	53.91
				
Dose (kGy)	G_0 (Pa)	G_1 (Pa)	η_1 (Pa·s)	R^2
60	0.0769	0.0650	2.63	0.9979
120	0.1343	0.3725	10.86	0.9981
180	0.1920	0.7171	26.30	0.9995
				

Parameters J_0, J_1, and λ_1 decrease with dose. Parameters η_0, G_0, G_1, and η_1 increase with dose. This trend was observed for both copolymers.

Table 3. Parameters from creep analysis of EVA 212 by four-parameter model. Embedded trends were created in Excel with Sparkline function.

EVA 212				
Dose (kGy)	J_0 $\left(\mathrm{Pa}^{-1}\right)$	J_1 $\left(\mathrm{Pa}^{-1}\right)$	λ_1 (s)	η_0 (Pa·s)
60	12.70	8.925	31.84	32.05
120	5.34	2.150	29.75	45.08
180	4.17	1.208	27.63	100.2
				
Dose (kGy)	G_0 (Pa)	G_1 (Pa)	η_1 (Pa·s)	R^2
60	0.0787	0.1121	3.568	0.9972
120	0.1874	0.4652	13.84	0.9995
180	0.2396	0.8280	22.88	0.9992
				

Figure 13 illustrates parameters derived from a quantitative analysis of experimental creep data obtained at 150 °C. Instantaneous creep compliance J_0 (see Figure 13a) represented by a spring in the model corresponds to the immediate deformation upon the application of stress. Although termed "instantaneous", this initial deformation took approximately 3 s in the experiment and is directly related to the degree of crosslinking. A higher level of crosslinking restricts significant rapid stretching, resulting in a lower J_0. As shown, J_0 decreases exponentially with increasing irradiation dose and is lower for EVA 212.

Zero-shear viscosity η_0 (see Figure 13b), represented by a dashpot in the model, signifies the material's resistance to a continuous, irreversible flow over time. A higher η_0 indicates a greater resistance to flow and ultimately leads to a smaller overall creep compliance. The data reveal that η_0 increases with increasing irradiation dose and is higher for EVA 212.

The lower instantaneous creep compliance J_0 and higher zero-shear viscosity η_0 observed for EVA 212 suggest a higher degree of crosslinking in this material compared to EVA 206 under the tested conditions.

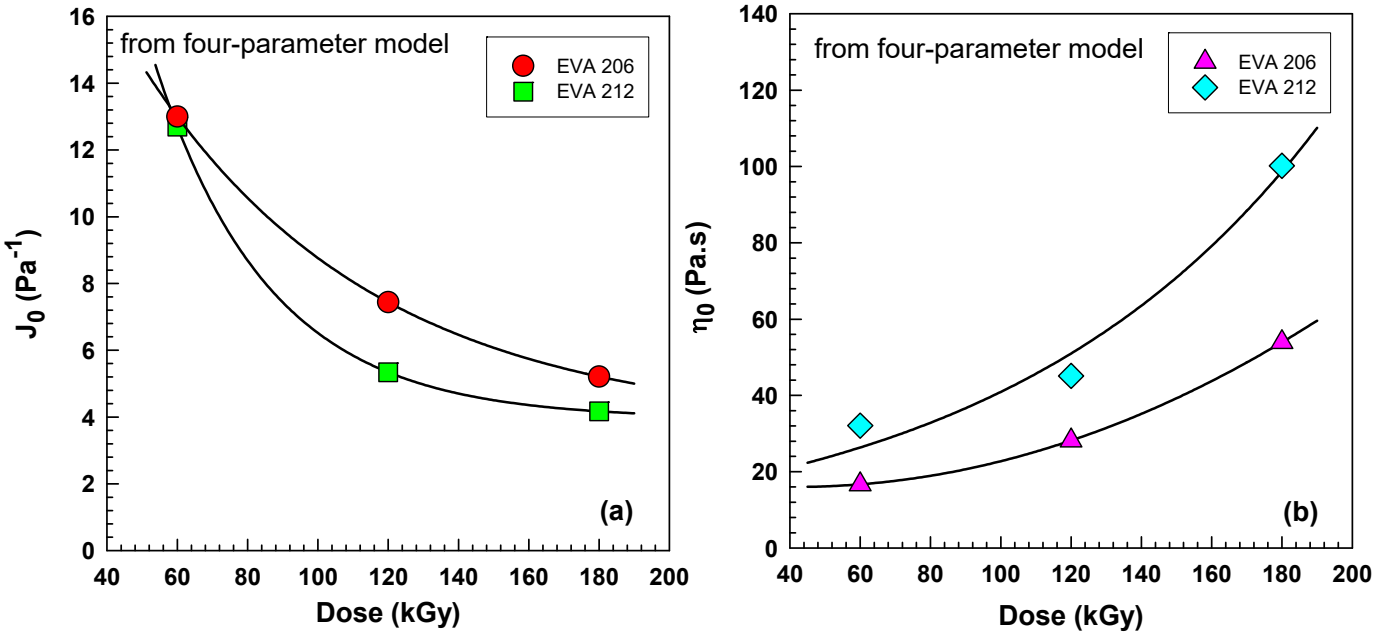

Figure 13. (**a**) Instantaneous creep compliance J_0 as a function of dose derived from the four-parameter model and (**b**) zero-shear viscosity η_0 as a function of dose derived from the four-parameter model for EVA 206 and EVA 212 tested at 150 °C.

The four-parameter viscoelastic model contains a Kelvin model, which describes the time-dependent viscoelastic behavior of the material. The Kelvin model consists of a spring and a dashpot connected in parallel. The spring element represents the elastic component, allowing for deformation up to a certain limit, while the dashpot represents the viscous component, resisting the rate of deformation. Upon removal of the stress, the Kelvin model predicts a complete recovery to the original shape.

In this context, the spring's stiffness, represented by the parameter G_1 (viscoelastic shear modulus—Figure 14a), indicates the material's resistance to deformation. Similarly, the parameter η_1 (viscoelastic shear viscosity—Figure 14b) represents the material's resistance to the rate of deformation. Higher values of both G_1 and η_1 signify a greater resistance to creep and are directly related to the level of crosslinking within the material. Increased crosslinking leads to higher values for both parameters.

Figure 14 demonstrates that the viscoelastic shear modulus G_1 increases almost linearly with increasing irradiation dose and is higher for EVA 212. Likewise, the viscoelastic shear viscosity η_1 also increases with irradiation dose and is higher for EVA 212. These trends in both G_1 and η_1 suggest a higher level of crosslinking in EVA 212 compared to EVA 206.

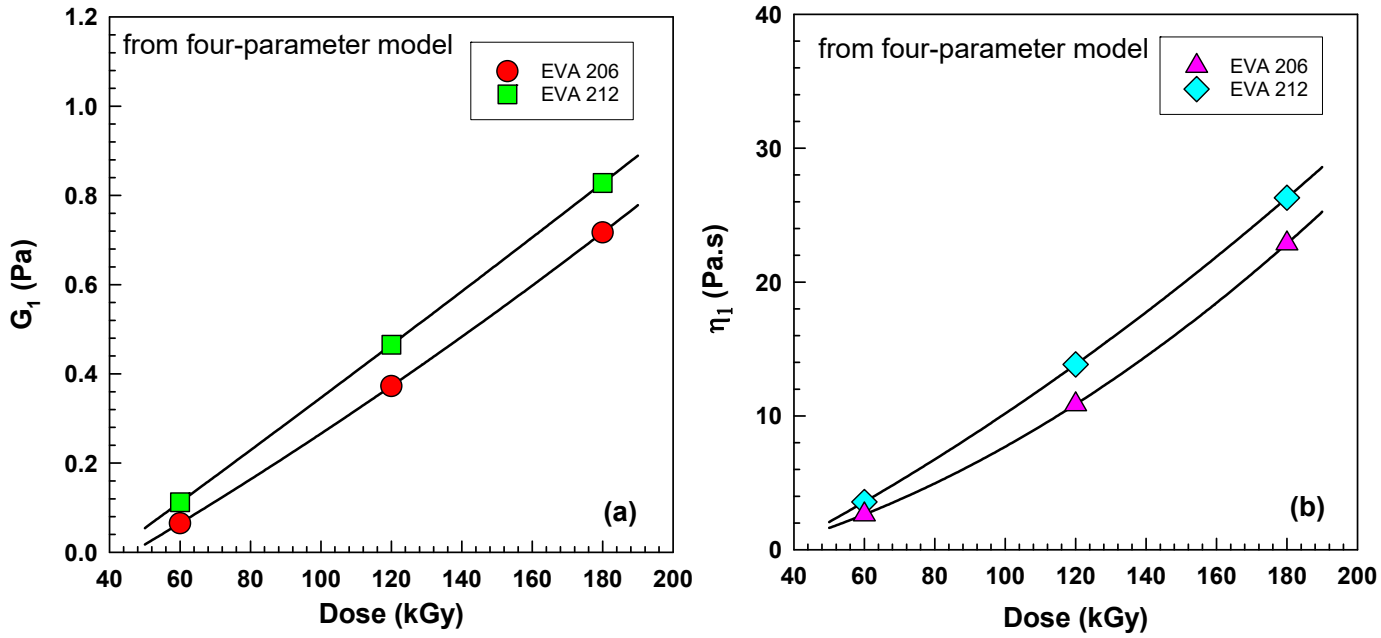

Figure 14. (**a**) Viscoelastic shear modulus G_1 as a function of dose derived from the four-parameter model and (**b**) viscoelastic shear viscosity η_1 as a function of dose derived from the four-parameter model for EVA 206 and EVA 212 tested at 150 °C.

Table 4. Parameters from creep analysis of EVA 206 by six-parameter model. Embedded trends were created in Excel with Sparkline function. Part 1.

EVA 206				
Dose (kGy)	J_0 $\left(\text{Pa}^{-1}\right)$	J_1 $\left(\text{Pa}^{-1}\right)$	λ_1 (s)	J_2 $\left(\text{Pa}^{-1}\right)$
60	15.43	7.705	49.63	5.388
120	6.786	2.296	54.33	1.471
180	4.907	1.383	61.55	0.6085
Dose (kGy)	λ_2 (s)	η_0 (Pa·s)	R^2	
60	5.251	47.71	0.9997	
120	4.855	50.16	0.9999	
180	4.742	57.33	0.9999	

Table 5. Parameters from creep analysis of EVA 212 by six-parameter model. Embedded trends were created in Excel with Sparkline function. Part 1.

EVA 212				
Dose (kGy)	J_0 $\left(\mathrm{Pa}^{-1}\right)$	J_1 $\left(\mathrm{Pa}^{-1}\right)$	λ_1 (s)	J_2 $\left(\mathrm{Pa}^{-1}\right)$
60	11.01	7.797	51.74	4.138
120	4.842	2.015	55.17	1.180
180	3.921	1.024	65.06	0.6218
	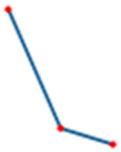			
Dose (kGy)	λ_2 (s)	η_0 (Pa·s)	R^2	
60	5.927	38.20	0.9997	
120	5.125	49.76	0.9998	
180	4.887	108.1	0.9998	
				

Instantaneous creep J_0 is much smaller for EVA 212 (for 60 kGy); its values are 15.43 for EVA 206 in Table 4 vs. 11.01 for EVA 212 in Table 5. The instantaneous jump J_0 indicates the elastic property and is reversible upon the removal of the applied stress [35]. At the same time, G_0 values (modulus) are higher for EVA 212.

The coefficient of determination R^2 values in Tables 4 and 5 were much closer to 1 in comparison to the four-parameter model. Double the value of 0.9999 was attained. The six-parameter model fitted the experimental data better. Sharma et al. also observed a very good fit to the experimental data with the six-parameter model [33].

Table 6. Parameters from creep analysis of EVA 206 by six-parameter model. Embedded trends were created in Excel with Sparkline function. Part 2.

EVA 206			
Dose (kGy)	G_0 (Pa)	G_1 (Pa)	η_1 (Pa·s)
60	0.06480	0.1298	6.442
120	0.1474	0.4355	23.66
180	0.2038	0.7230	44.50
			
Dose (kGy)	G_2 (Pa)	η_2 (Pa·s)	
60	0.1856	0.9745	
120	0.6800	3.301	
180	1.643	7.793	
			

Table 7. Parameters from creep analysis of EVA 212 by six-parameter model. Embedded trends were created in Excel with Sparkline function. Part 2.

EVA 212			
Dose (kGy)	G_0 (Pa)	G_1 (Pa)	η_1 (Pa·s)
60	0.09085	0.1283	7.076
120	0.2065	0.4963	32.29
180	0.2550	0.9768	50.54
			
Dose (kGy)	G_2 (Pa)	η_2 (Pa·s)	
60	0.2417	1.432	
120	0.8475	4.085	
180	1.608	7.859	
			

3.5. Room-Temperature Stress–Strain

Figure 15 displays the room-temperature stress–stain curves evaluated in the dynamic mechanical analyzer in shear mode for various irradiation levels. The initial slope of the curves represents the shear modulus, denoted as G and measured in MPa. EVA 212 exhibits lower G values, indicating that it is softer and more prone to yielding. This observation aligns with the Escorene product literature, which specifies tensile modulus (E) values of 110 MPa and 90 MPa for EVA 206 and 212, respectively. A higher vinyl acetate (VA) content disrupts the crystalline phase and increases the volume of the amorphous phase.

Interestingly, the shear modulus shows a decreasing trend with increasing irradiation, which is the opposite to the trend observed at 150 °C, as discussed in relation to Figure 18. It is likely that the electron beam irradiation caused some damage to the lamellar structure, which plays a significant role at lower temperatures. At these low temperatures, the crystal lamellae act as tie points for the amorphous chains, and their influence appears to be more important than that of chemical crosslinking.

This light crosslinking is crucial in the foaming industry. At high temperatures, above the melting point of EVA where foaming occurs, the chemical crosslinks aid in the foaming process by preventing bubble collapse. An optimal level of crosslinking is necessary to form bubbles of the correct size; excessive crosslinking hinders bubble growth, while insufficient crosslinking leads to their collapse. In the foaming industry, it is common practice to assess the level of crosslinking using high-temperature tests (e.g., 150 °C). Low-temperature tests (25 °C) do not effectively reveal subtle differences in crosslinking levels, because physical crosslinking is significantly stronger than chemical crosslinking at these temperatures.

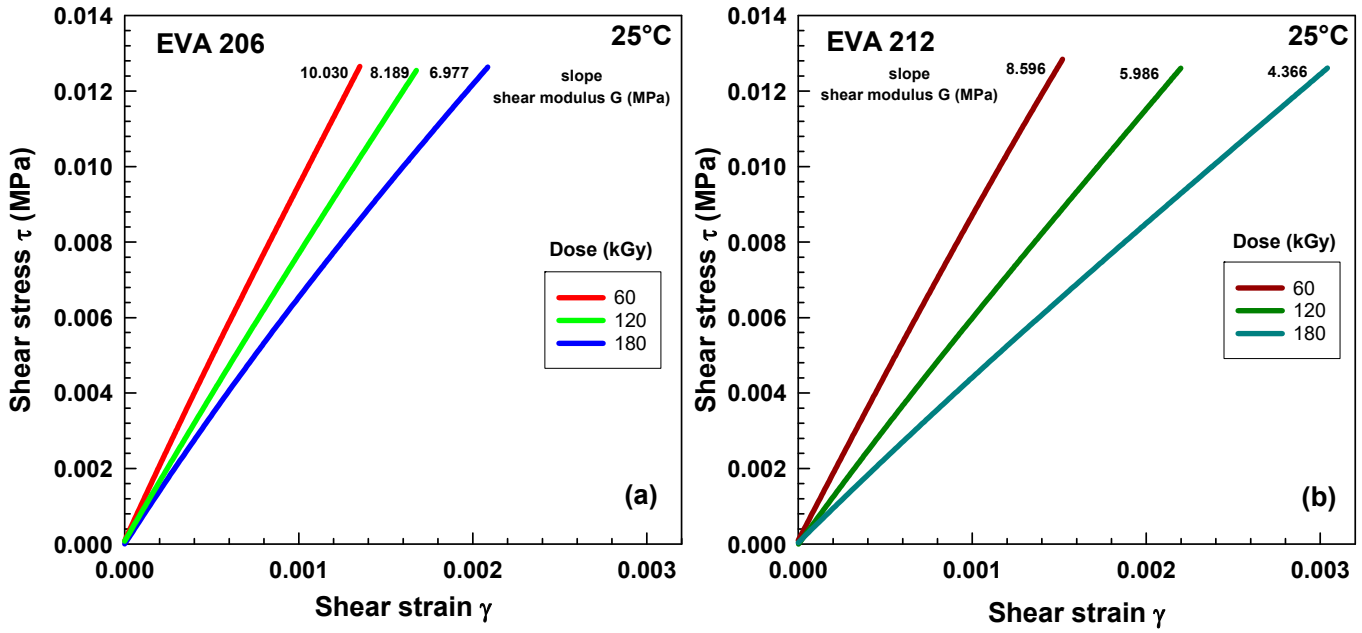

Figure 15. Shear stress versus shear strain measured by DMA at room temperature for samples irradiated by 60, 120, and 180 kGy: (**a**) EVA 206, (**b**) EVA 212.

3.6. High-Temperature Stress–Strain

Stress–strain curves are illustrated in Figure 16. A higher level of irradiation gives a higher slope (60, 120, and 180 kGy—red, green, and blue curves). Stress increases with a higher content of VA for the same strain, implying a higher modulus (compare light red to dark red, light green to dark green, and light blue to dark blue). The higher VA content causes a higher level of crosslinking, i.e., higher modulus.

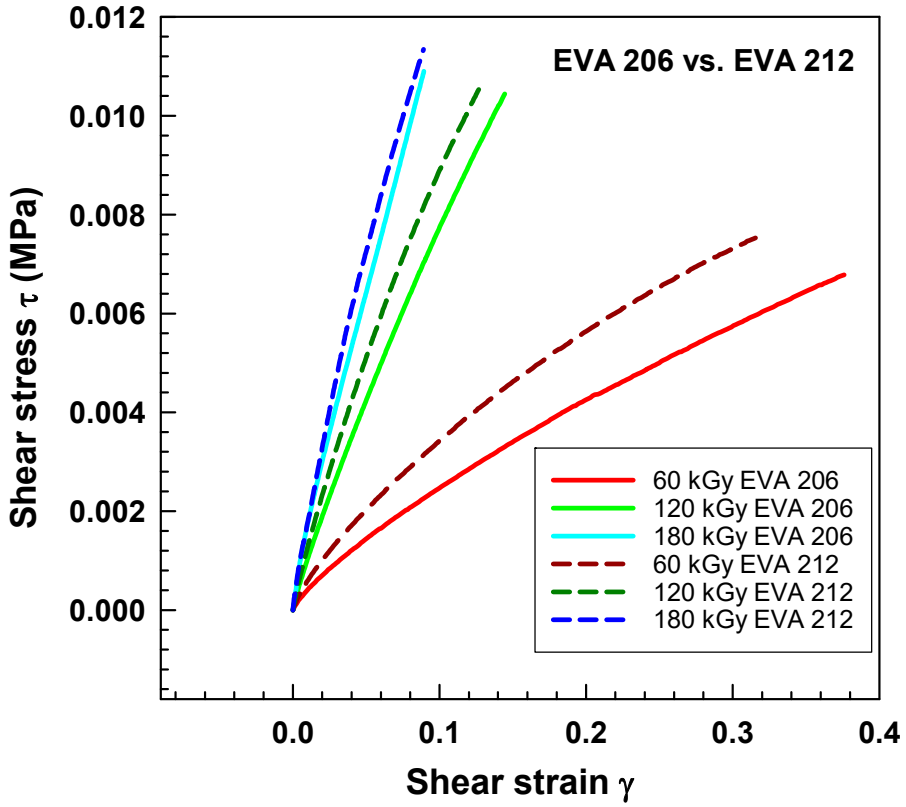

Figure 16. Stress–strain curves of EVA copolymers measured by DMA at 150 °C.

In the rubber industry, it is common practice to observe stress at 100 and at 300%, so-called M100 and M300. For plastics tested at room temperature, it is common to observe a slope at the initial part of the curve, i.e., Young's modulus. Our measurement takes place at 150 °C, the sample is crosslinked, and its behavior during the stress–strain test resembles more rubber. Therefore, we chose to compare the stress values at a strain of 0.03 (Figure 17). The differences are very clear using this method.

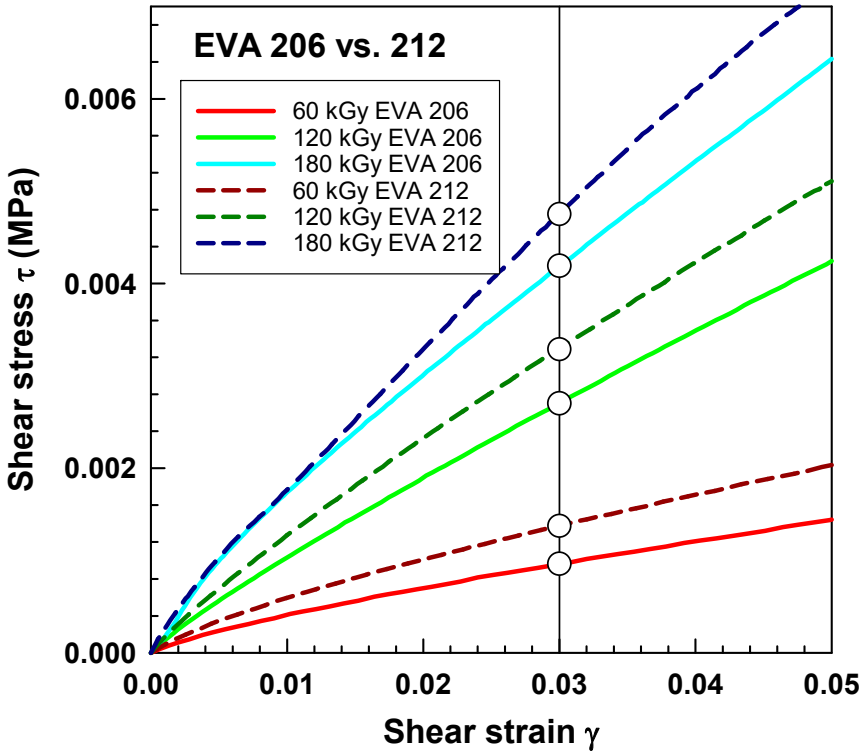

Figure 17. Tensile stress–strain curves with determination of stress at 0.03 strain represented by white dots.

Figure 18 illustrates an increase in stress with dose. EVA 212 has higher levels of stress than EVA 206 does, corresponding well with higher crosslinking.

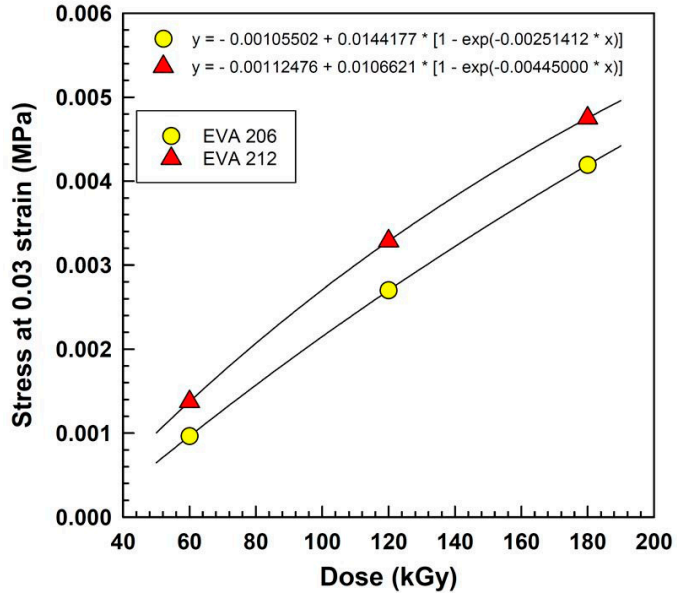

Figure 18. Trends of stress at a strain of 0.03 vs. dose.

Figure 19a depicts the frequency sweep data of viscosity as a function of frequency in logarithmic form according to Equation (4). There are three lines representing three levels of radiation. With increasing frequency, $log|\eta^*|$ linearly decreases with $log f$. With increasing radiation, the viscosities increase significantly, especially at low frequencies. This is the reason behind the increasing shear thinning parameter n listed as a slope of the lines. Figure 19b shows the pre-exponential factor k increasing almost perfectly linearly with increasing irradiation level. Our data are in agreement with McNally et al. [45], Durmus et al. [38], Datta et al. [46], and Shin et al. [47].

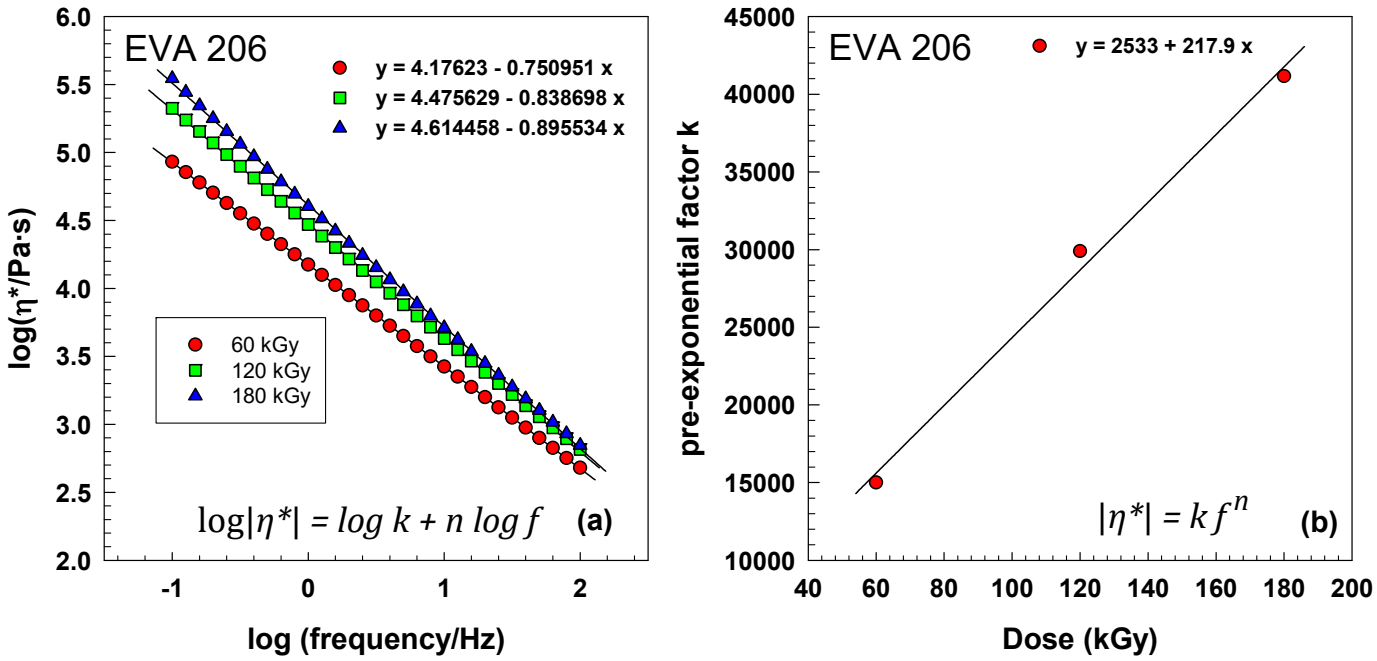

Figure 19. (**a**) The complex viscosity as a function of frequency, and (**b**) the pre-exponential factor k.

Figure 20 illustrates the storage shear modulus G' and loss modulus G'' as a function of frequency. Both moduli exhibit a linear increase with frequency when plotted on logarithmic coordinates. Figure 20a shows the results for EVA 206 while Figure 20b illustrates results for EVA 212.

In a typical entangled polymer system, G' is observed to be higher than G''. G' represents the elastic part of the modulus, which grows with increasing crosslinking. However, for the irradiated crosslinked system under investigation, G'' values exceed those of G'. The storage shear modulus (G') represents the elastic component, which increases with the degree of crosslinking. The G' values are marginally elevated for EVA 212 at 60 kGy, potentially indicating a higher crosslinking density. These results are consistent with observations reported by Bai et al. [48], Kraft et al. [49], and Barron and Macosko [50]. The slopes of the linear fits are lower for EVA 212, and the coefficients of determination R^2 are approximately 0.999, with one instance reaching even 0.9999, signifying a strong correlation between the experimental data and the linear model. We have observed different trends for room temperature results compared to high temperature results. Therefore, we were compelled to search the literature and compare our results to other researchers. This comparison is listed in Appendix C.

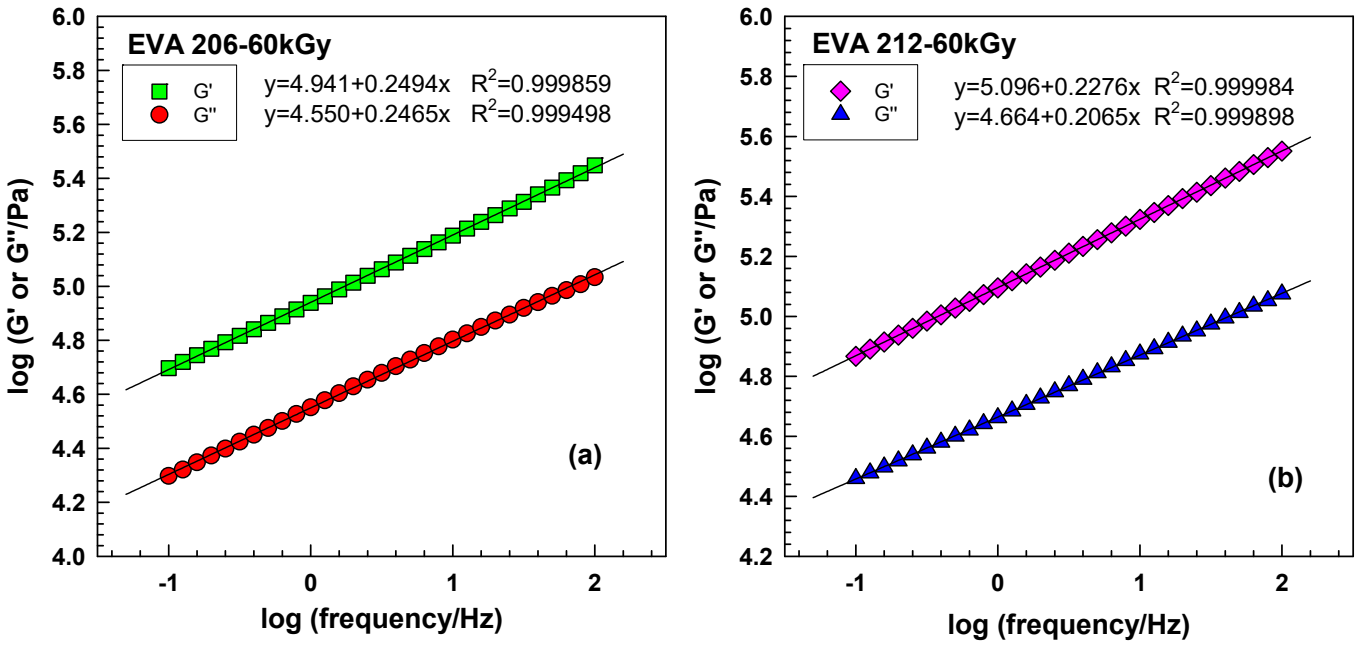

Figure 20. Storage shear modulus G' and loss modulus G'' as a function of frequency in logarithmic coordinates: (**a**) EVA 206-60 kGy, (**b**) EVA 212-60 kGy.

4. Conclusions

This study clarified the influence of electron beam irradiation on the mechanical behavior of ethylene-vinyl acetate (EVA) copolymers with varying vinyl acetate (VA) content (6 wt.% and 12 wt.%). Irradiation doses ranging from 60 to 180 kGy were applied, and the resulting changes in creep, frequency sweep, and stress–strain characteristics were assessed at 25 °C and 150 °C using the dynamical mechanical analyzer (DMA). The viscoelastic response was quantitatively evaluated using four-parameter and six-parameter models. The following conclusions are drawn:

1. **Crosslinking and Creep Resistance:** Electron beam irradiation effectively induced crosslinking, as evidenced by a progressive decrease in creep compliance with increasing irradiation dose at high temperature. EVA 212, exhibiting a higher VA content, exhibited a lower instantaneous creep compliance J_0 and reduced creep after five minutes compared to EVA 206, indicating a greater degree of crosslinking and enhanced resistance to time-dependent deformation. Meanwhile, for room temperature, the trend was the opposite, which was explained by damage to the crystalline phase and fewer entanglements and a decrease in the number and effectiveness of tie molecules.
2. **Viscoelastic Properties:** The Newtonian viscosity η_0 and instantaneous shear modulus G_0 increased with irradiation dose, signifying a reduction in material flow and enhanced rigidity. EVA 212 displayed higher η_0 and G_0 values, further confirming the beneficial impact of higher VA content on high-temperature mechanical stability.
3. **Model Accuracy:** The six-parameter model demonstrated superior accuracy in describing the creep behavior, achieving a coefficient of determination R^2 of 0.9997 for EVA 212 irradiated at 60 kGy, compared to the four-parameter model's lower R^2 value (e.g., 0.9972). This confirms the better accuracy of the six-parameter model compared to the four-parameter model.

4. **Stress–Strain Behavior:** Shear stress at a strain of 0.03 increased with irradiation dose and was greater for EVA 212, confirming the observed increase in shear modulus and indicating enhanced crosslinking. Again, the room-temperature modulus decreased with irradiation due to damaged crystalline lamellae and damaged tie molecules between lamellae.
5. **Overall Impact of Irradiation:** Electron beam irradiation significantly enhanced the high-temperature mechanical properties of both EVA copolymers. The irradiation-induced crosslinking resulted in increased resistance to deformation and creep at elevated temperature, with EVA 212 consistently exhibiting superior performance, highlighting the importance of VA content in tailoring the high-temperature behavior of irradiated EVA copolymers.

Author Contributions: Writing—original draft preparation, A.S.; supervision, P.S. All authors have read and agreed to the published version of the manuscript.

Funding: This research was funded by the Department of Polymer Engineering, Faculty of Technology, Tomas Bata University, Zlin, grant number IGA/FT/2024/008.

Data Availability Statement: The data that support the findings of this work are available from the corresponding author upon reasonable request.

Conflicts of Interest: The authors declare no conflicts of interest.

Abbreviations

The following abbreviations are used in this manuscript:

MDPI	Multidisciplinary Digital Publishing Institute
EVA	Ethylene-vinyl acetate
VA	Vinyl acetate
MFI	Melt flow index
EB	Electron beam
DMA	Dynamic mechanical analyzer
DSC	Differential scanning calorimetry
WAXD	Wide-angle X-ray diffraction
N/A	Not applicable

Appendix A

Depending on the nature of the polymer, various crosslinking methods (Table A1) can be used. During the crosslinking process, the active functional groups of polymer chains react chemically or physically with the crosslinking agent and a three-dimensional network is formed.

Crosslinking can occur through the polymerization of monomers with more than two functional groups (by condensation) or by irradiation of the polymer chain between covalent bonds, vulcanization with sulfur, or chemical reactions by adding various chemicals in combination with heating and sometimes pressure. A monomeric unit containing two or more functional groups (double bonds or functional groups) is called a crosslinking agent or crosslinker. A crosslinker may contain two, three, or four crosslinking sites. In all cases, the chemical structure of the polymer is altered by the crosslinking process [15].

Table A1. An overview of crosslinking methods.

Crosslinking Method	Crosslinker	Advantages	Disadvantages	Applications
Polymerization of Monomers	Monomers with 2+ functional groups (e.g., diacrylate, diisocyanates, glutaraldehyde, formaldehyde), free-radical polymerization	Flexible, widely used	Limited to certain functional groups, need for specific conditions (e.g., radical initiators)	Coatings, adhesives, thermoset resins
Irradiation (Electron Beam or UV)	Cobalt-60, electron beam, UV light	High precision, fast process, no need for chemical crosslinkers	High energy cost, limited penetration depth in thick materials	Medical devices, cable insultation, packaging materials
Vulcanization (Sulfur Crosslinking)	Sulfur (e.g., elementary sulfur)	Effective for rubber, enhances elasticity, well-established process	Requires high temperature, produces sulfur compounds, can be slow	Tires, rubber products, seals
Chemical Crosslinking	Peroxides, silanes, polyisocyanates	Chemical cross-linking is much stronger and stable towards heat, mechanical, or any other action	Cross-linking is irreversible and cannot be reversed. Requires careful handling of chemicals, may need high temperature	Adhesives, coatings, elastomers, engineering plastics
Thermal Crosslinking	Heat-activated initiator, peroxides	Simple, efficient for thermoset polymers, good for large-scale applications	May require high temperatures, limited to heat-resistant materials	Electronics, automotive, aerospace applications
Pressure-Chemical Crosslinking	Crosslinkers + heat and pressure	High precision, can create durable and robust materials	Requires special equipment for the high-pressure expensive process	Aerospace composites, high-strength thermoset resins, moldings
Physical Crosslinking	Physical interactions (e.g., hydrogen bonding, ionic crosslinks)	No need for chemical crosslinkers, reversible, adaptable	Weaker bonds, less stable under certain conditions	Hydrogels, responsive materials, membranes
Biological Crosslinking	Enzymes (e.g., transglutaminase), glutaraldehyde	Biocompatible, can be specific, and mild conditions	Limited control over crosslinking density, may need specific conditions	Medical devices, tissue engineering, drug delivery system

Appendix B

R-squared is referred to as the coefficient of determination R^2 as a measure of how well a linear regression model fits a dataset. It represents the proportion of the variance in the response variable that can be perfectly explained by the predictor variable.

The value for R-squared can range from 0 to 1. A value of 0 indicates that the response variable cannot be explained by the predictor variable at all. A value of 1 indicates that the response variable can be perfectly explained without error by the predictor variable.

Using SSR and SST, we can calculate R-squared as

$$R^2 = \frac{SSR}{SST} \tag{A1}$$

where SSR is the Sum of Squares Regression and SST is the Sum of Squares Total.

For the four-parameter model, we used the following equations:

$$J(t) = \frac{1}{G_0} + \frac{1}{G_1}\left[1 - exp\left(\frac{-tG_1}{\eta_1}\right)\right] + \frac{t}{\eta_0} \tag{A2}$$

$$f = y_0 + a \cdot [1 - \exp(-b \cdot x)] + c \cdot x \tag{A3}$$

$$y_0 = \frac{1}{G_0}\, G_0 = \frac{1}{y_0}$$
$$a = \frac{1}{G_1}\, G_1 = \frac{1}{a}$$
$$b = \frac{G_1}{\eta_1}\, \eta_1 = \frac{G_1}{b}$$
$$c = \frac{1}{\eta_0}\, \eta_0 = \frac{1}{c}$$

For the six-parameter model, we used the following equations:

$$J(t) = \frac{1}{G_0} + \frac{1}{G_1}\left[1 - exp\left(\frac{-tG_1}{\eta_1}\right)\right] + \frac{1}{G_2}\left[1 - exp\left(\frac{-tG_2}{\eta_1}\right)\right] + \frac{t}{\eta_0} \quad \text{(A4)}$$

$$f = y_0 + a{\cdot}[1 - \exp(-b{\cdot}x)] + c{\cdot}[1 - \exp(-d{\cdot}x)] + e{\cdot}x \quad \text{(A5)}$$

$$y_0 = \frac{1}{G_0}\, G_0 = \frac{1}{y_0}$$
$$a = \frac{1}{G_1}\, G_1 = \frac{1}{a}$$
$$b = \frac{G_1}{\eta_1}\, \eta_1 = \frac{G_1}{b}$$
$$c = \frac{1}{G_2}\, G_2 = \frac{1}{c}$$
$$d = \frac{G_2}{\eta_2}\, \eta_2 = \frac{G_2}{d}$$
$$e = \frac{1}{\eta_0}\, \eta_0 = \frac{1}{e}$$

Example of calculation of molar ratio for EVA 206—6 wt.% of vinyl acetate
100 g EVA: 6 g VA, 94 g ET.

Ethylene = —CH_2—CH_2—, $M_{ET} = 2{\cdot}C + 4{\cdot}H = 2{\cdot}12.011 + 4{\cdot}1.008 = 28.054$ g/mol

Vinyl acetate = $C_4H_6O_2$, $M_{VA} = 4{\cdot}C + 6{\cdot}H + 2{\cdot}O = 4{\cdot}12.011 + 6{\cdot}1.008 + 2{\cdot}16 = 86.092$ g/mol

$$n_{VA} = \frac{m_{VA}}{M_{VA}} = \frac{6}{86.092} = 0.0696924 \text{ mol}$$
$$n_{ET} = \frac{m_{ET}}{M_{ET}} = \frac{94}{28.054} = 3.35068 \text{ mol}$$
$$\frac{n_{ET}}{n_{VA}} = \frac{3.35068}{0.0696924} = 48.1 = \frac{48}{1}$$
$$\frac{n_{VA}}{n_{ET}} = \frac{0.0696924}{3.35068} = 0.02$$

ET: 48.0778 mol.
VA: 1 mol.

$$m_{ET} = n{\cdot}M = 48.0778{\cdot}28.054 = 1348.7746$$
$$m_{VA} = n{\cdot}M = 1{\cdot}86.092 = 86.0920$$
$$1434.8660 + 86.092 = 1434.8660$$

wt. fraction:

$$\frac{86.0920}{1434.8660} = 0.06$$

Example of calculation of molar ratio for EVA 212—12 wt.% of vinyl acetate
100 g EVA: 12 g VA, 88 g ET.

$$\text{Ethylene} = —CH_2—CH_2—,\ M_{ET} = 2{\cdot}C + 4{\cdot}H = 2{\cdot}12.011 + 4{\cdot}1.008 = 28.054 \text{g/mol}$$

$$\text{Vinyl acetate} = C_4H_6O_2,\ M_{VA} = 4{\cdot}C + 6{\cdot}H + 2{\cdot}O = 4{\cdot}12.011 + 6{\cdot}1.008 + 2{\cdot}16 = 86.092 \text{ g/mol}$$

$$n_{VA} = \frac{m_{VA}}{M_{VA}} = \frac{12}{86.092} = 0.139386 \text{ mol}$$

$$n_{ET} = \frac{m_{ET}}{M_{ET}} = \frac{88}{28.054} = 3.13681 \text{ mol}$$

$$\frac{n_{ET}}{n_{VA}} = \frac{3.13681}{0.139386} = 22.5 = \frac{23}{1}$$

$$\frac{n_{VA}}{n_{ET}} = \frac{0.139386}{3.13681} = 0.04$$

ET: 22.504 mol.
VA: 1 mol.

$$m_{ET} = n{\cdot}M = 22.504{\cdot}28.054 = 631.327$$

$$m_{VA} = n{\cdot}M = 1{\cdot}86.092 = 86.0920$$

$$631.327 + 86.092 = 717.417$$

wt. fraction:

$$\frac{86.0920}{717.417} = 0.12$$

Appendix C

Our results showed different trends for high-temperature tests compared to room-temperature tests. Therefore, we searched the literature for what other researchers wrote about the influence of electron beam irradiation on the crosslinking of EVA copolymers and their blends and the influence of crosslinking on various room-temperature and high-temperature properties. They are summarized in Table A2.

Ramarad et al. [51] examined the improvement in the properties of reclaimed waste tire rubber by blending with poly(ethylene-co-vinyl acetate) and electron beam irradiation. They studied blends and also pure EVA exposed to electron beam irradiation in the range of 0–200 kGy. This EVA had 18% of VA, an MFI of 2.3 g/10 min, and a density of 0.947 g/cm^3.

Sabet and Soleimani [18] studied the impact of electron beam irradiation in the range of 0–260 kGy on low-density polyethylene and ethylene vinyl acetate with 18% of VA.

Wang et al. [52] researched the effect of electron beam irradiation on the physical properties of ethylene-vinyl acetate copolymer composites. EVA had 28 wt.% of VA. The composites also contained cellulose acetate butyrate and polyamide 6. Irradiation doses were selected in the range of 40–300 kGy.

Munusamy et al. [53] analyzed the effect of electron beam irradiation on the properties of ethylene vinyl acetate copolymer/natural rubber/organoclay nanocomposites. EVA contained 15% of VA, and the electron beam irradiation was in the range of 0–200 kGy.

Michael et al. [54] explored the effect of electron beam irradiation on (waste tire dust)-filled ethylene vinyl acetate in the presence of bisphenol a diglycidyl ether. EVA had 15 wt.% of VA, an MFI of 1.5 g/10 min, and a density of 0.93 g/cm^3, and the electron beam irradiation was in the range of 0–200 kGy.

Hwang et al. [55] studied the effect of electron beam irradiation on the dispersion and properties of poly(ethylene-co-vinyl acetate)/clay nanocomposites. EVA had 31 wt.% of VA, and the electron beam irradiation was in the range of 20–200 kGy.

Rezaeian et al. [56] probed the improvements in physical and mechanical properties of electron beam irradiation-crosslinked EVA foams. EVA had 18 wt.% of VA, an MFI of 2.1 g/10 min, and a density of 0.93 g/cm^3, and the electron beam irradiation was in the range of 40–80 kGy.

Gad [57] examined the improvement in the properties of poly(ethylene-co-vinyl acetate)/clay composite by using electron beam irradiation. The electron beam irradiation was in the range of 0–250 kGy.

Matsui et al. [58] investigated mechanical changes in the electron-beam irradiated ethylene vinyl-acetate copolymer. EVA had 5, 9, and 15 wt.% of VA. The electron beam irradiation was in the range of 0–200 kGy.

Dutta et al. [42] analyzed the effect of electron beam irradiation on the creep response of EVA/TPU blends. EVA contained 28% of vinyl acetate, its MFI was 3 g/10 min at 190 °C (2.6 kg load), and its density was 0.95 g/cm^3. The electron beam irradiation was in the range of 0–200 kGy.

Hamid et al. [59] researched the influence of electron beam irradiation on the high-temperature mechanical properties of ethylene vinyl acetate/carbon fiber composites. EVA contained 28 wt.% of vinyl acetate, its MFI was 3.0 g/10 min, and its density was 0.951 g/cm^3. The electron beam irradiation was in the range of 60–180 kGy.

Zhang et al. [6] studied crosslinked poly(ethylene-vinyl acetate) with 28 wt.% of VA. They measured the creep at 180 °C.

Hui et al. [60] probed the influence of the crosslinking of EVA on high-temperature creep resistance. EVA contained 18 wt.% of VA.

Qi et al. [61] examined the high-temperature creep of crosslinked EVA fibers. EVA contained 18 wt.% of VA and had an MFI of 2.5 g/10 min.

Table A2. Comparison of trends in other research to our results. Influence of e-beam radiation on various properties of EVA reported by various researchers.

Property	UP	DOWN	MAXIMUM	Our Results
Tensile strength	[53,56]		[18,42,51,52,54,55,57,58]	N/A
Elongation at break		[18,42,51,52,54–57]	[53]	N/A
Modulus	[42,53,55]	[51]	[54]	DOWN
Tear strength			[51]	N/A
Hardness	[54]	[51]	[18,57]	N/A
Gel content	[18,52–59]			N/A
Density		[18]		N/A
Crystallinity		[58]		DOWN
Complex viscosity	[42]			UP
Complex modulus	[42]			UP
Creep compliance		[42]		UP
Crosslink density	[42]			UP
High-temperature creep		[6,59–61]		DOWN
High-temperature modulus	[6,59]			UP

N/A—not applicable. UP—increasing trend. DOWN—decreasing trend. All properties were at room temperature except for the last two rows.

References

1. Barnes, S.E.; Brown, E.C.; Sibley, M.G.; Edwards, H.G.M.; Coates, P.D. Vibrational spectroscopic and ultrasound analysis for the in-process monitoring of poly(ethylene vinyl acetate) copolymer composition during melt extrusion. *Analyst* **2005**, *130*, 286–292. [CrossRef]

2. Qin, H.J.; Zhang, T.W.; Bao, L.H.; Dang, B.; Li, J.X. Rapid Synthesis of Molybdenum Disulfide@Ferric Oxide Nanomaterials Using Gamma Rays for the Efficient Improvement of the Flame Retardancy and Mechanical Properties of EVA/Magnesium Hydroxide Composites. *J. Appl. Polym. Sci.* **2025**, *142*, e56831. [CrossRef]
3. Liang, J.Y.; Wu, J.H.; Wang, C.H.; Sang, J.; Ren, K.S.; Ngai, T.; Lin, W. Ethylene vinyl acetate as a multifunctional compatibilizer for natural rubber/-1,4-polybutadiene rubber blends with enhanced compatibility, filler dispersion and mechanical properties. *Collagen Leather* **2025**, *7*, 3. [CrossRef]
4. Zia-ul-Haq, M.; Wu, J.; Peng, Z.L.; Zhang, Y. Mechanical properties and thermal stability of modified calcium sulfate whisker-reinforced polydimethylsiloxane/ethylene-vinyl acetate copolymer composites. *Iran. Polym. J.* **2023**, *32*, 1335–1346. [CrossRef]
5. Mendoza-Duarte, M.E.; Roacho-Pérez, J.A.; Reyes, A.G.Q.; Garza-Treviño, E.N.; Sánchez-Domínguez, C.N.; García-Casillas, P.E.; Vega-Rios, A. Poly(Ethylene-Vinyl Acetate)-Poly(Lactic Acid)-Poly(Styrene-Methyl Methacrylate) Blends: Study of Mechanical Properties Under Hydrolytic Degradation and Cytotoxic Evaluation. *J. Polym. Environ.* **2023**, *32*, 1217–1232. [CrossRef]
6. Zhang, J.C.; Li, X.P.; Zhang, S.B.; Zhu, W.Q.; Li, S.H.; Zhang, Y.J.; Hu, Y.M.; Zhou, G.Y. Facile Approach for the Preparation of Robust and Thermally Stable Silyl Ether Cross-Linked Poly(ethylene-vinyl acetate) Vitrimers. *ACS Appl. Polym. Mater.* **2023**, *5*, 8379–8386. [CrossRef]
7. Lunchev, A.V.; Kashcheev, A.; Tok, A.L.Y.; Lipik, V. Impact of hollow glass microsphere addition to poly(ethylene vinyl) acetate foam on mechanical properties of sports footwear. *J. Appl. Polym. Sci.* **2023**, *140*, e54084. [CrossRef]
8. Luna, C.B.B.; Ferreira, E.D.B.; Siqueira, D.D.; dos Santos, E.A.; Araújo, E.M. Additivation of the ethylene-vinyl acetate copolymer (EVA) with maleic anhydride (MA) and dicumyl peroxide (DCP): The impact of styrene monomer on cross-linking and functionalization. *Polym. Bull.* **2022**, *79*, 7323–7346. [CrossRef]
9. McLoughlin, K.M.; Oskouei, A.J.; Sing, M.K.; Bandegi, A.; Mitchell, S.; Kennedy, J.; Gray, T.G.; Manas-Zloczower, I. Thermomechanical Properties of Cross-Linked EVA: A Holistic Approach. *ACS Appl. Polym. Mater.* **2023**, *5*, 1430–1439. [CrossRef]
10. Chong, L.K.; Osman, A.F.; Fauzi, A.A.A.; Alrashdi, A.A.; Halim, K.A.A. The Mechanical and Thermal Properties of Poly(ethylene-co-vinyl acetate) (PECoVA) Composites with Pristine Dolomite and Organophilic Microcrystalline Dolomite (OMCD). *Polymers* **2021**, *13*, 3034. [CrossRef]
11. Zhao, Y.; Peng, K.Y.; Xi, J.X.; Shahab, S.; Mirzaeifar, R. Achieving multimodal locomotion by a crosslinked poly(ethylene-co-vinyl acetate)-based two-way shape memory polymer. *Smart Mater. Struct.* **2022**, *31*, 015034. [CrossRef]
12. Hendriko, A.; Juwono, A.L.; Budiman, I.; Subyakto; Soegijono, B.; Sadir, M.; Sudarmanto; Purnomo, D.; Narto; Akbar, F.; et al. Mechanical and thermal properties of non-structural adhesive mortar using linear low-density polyethylene (LLDPE) aggregate substitution with vinyl acetate/ethylene (VAE) interface. *Colloid Polym. Sci.* **2024**, *302*, 539–560. [CrossRef]
13. Ahmed, J.; Mushtaq, S.; Adeel, M. Fabrication of ethylene-vinyl acetate copolymer/polyamide/modified sepiolite composite with improved physical properties via e-beam irradiation. *Radiat. Phys. Chem.* **2021**, *189*, 109779. [CrossRef]
14. Santana, J.G.; Akbulut, M.; Temperini, M.L.A.; Rangari, V.K.; Guven, O.; Moura, E. Synergistic effect of e-beam irradiation and graphene oxide incorporation on thermal, mechanical, and barrier properties of poly (ethylene-co-vinyl alcohol) film. *Radiat. Phys. Chem.* **2022**, *199*, 110343. [CrossRef]
15. Kolhe, A.; Chauhan, A.; Dongre, A. A Review on various methods for the Cross-linking of Polymers. *Res. J. Pharm. Dos. Forms Technol.* **2022**, *14*, 183–188. [CrossRef]
16. Rajawasam, C.W.H.; Dodo, O.J.; Weerasinghe, M.A.S.N.; Raji, I.O.; Wanasinghe, S.V.; Konkolewicz, D.; De Alwis Watuthanthrige, N. Educational series: Characterizing crosslinked polymer networks. *Polym. Chem.* **2024**, *15*, 219–247. [CrossRef]
17. Makuuchi, K.; Cheng, S. *Radiation Processing of Polymer Materials and Its Industrial Applications*; John Wiley & Sons, Inc.: Hoboken, NJ, USA, 2012.
18. Sabet, M.; Soleimani, H. The impact of electron beam irradiation on Low density polyethylene and Ethylene vinyl acetate. In Proceedings of the 5th International Conference on Nanomaterials and Materials Engineering (Icnme 2017), Bali, Indonesia, 1–3 April 2017; Volume 204. [CrossRef]
19. Khodkar, F.; Ebrahimi, N.G. Effect of Irradiation on Mechanical and Structural Properties of Ethylene Vinyl Acetate Copolymers Hollow Fibers. *J. Appl. Polym. Sci.* **2011**, *119*, 2085–2092. [CrossRef]
20. Alothman, O.Y. Processing and Characterization of High Density Polyethylene/Ethylene Vinyl Acetate Blends with Different VA Contents. *Adv. Mater. Sci. Eng.* **2012**, *2012*, 635693. [CrossRef]
21. Khonakdar, H.A.; Jafari, S.H.; Haghighi-Asl, A.; Wagenknecht, U.; Haussler, L.; Reuter, U. Thermal and mechanical properties of uncrosslinked and chemically crosslinked polyethylene/ethylene vinyl acetate copolymer blends. *J. Appl. Polym. Sci.* **2007**, *103*, 3261–3270. [CrossRef]
22. Gu, P.Z.; Zhang, J. Vinyl acetate content influence on thermal, non-isothermal crystallization, and optical characteristics of ethylene-vinyl acetate copolymers. *Iran. Polym. J.* **2022**, *31*, 905–917. [CrossRef]
23. G. Farias, G.M.; Agrawal, P.; Hanken, R.B.L.; de Araújo, J.P.; de Oliveira, A.D.B.; de Mélo, T.J.A. Effect of EVA copolymer containing different VA content on the thermal and rheological properties of bio-based high-density polyethylene/ethylene vinyl acetate blends. *J. Therm. Anal. Calorim.* **2021**, *146*, 2127–2139. [CrossRef]

24. Sethi, M.; Gupta, N.K.; Srivastava, A.K. Dynamic mechanical analysis of polyethylene and ethylene vinylacetate copolymer blends irradiated by electron beam. *J. Appl. Polym. Sci.* **2002**, *86*, 2429–2434. [CrossRef]
25. Chattopadhyay, S.; Chaki, T.K.; Bhowmick, A.K. Structural characterization of electron-beam crosslinked thermoplastic elastomeric films from blends of polyethylene and ethylene-vinyl acetate copolymers. *J. Appl. Polym. Sci.* **2001**, *81*, 1936–1950. [CrossRef]
26. Dutta, J.; Chatterjee, T.; Dhara, G.; Naskar, K. Exploring the Influence of Electron Beam Irradiation on the Morphology, Physico-mechanical, Thermal behaviour and Performance Properties of EVA and TPU Blends. *RSC Adv.* **2015**, *5*, 41563–41575. [CrossRef]
27. Wang, S.F.; Zhang, Y.; Zhang, Y.X.; Zhang, C.M.; Li, E.J. Crosslinking of polyvinyl chloride by electron beam irradiation in the presence of ethylene-vinyl acetate copolymer. *J. Appl. Polym. Sci.* **2004**, *91*, 1571–1575. [CrossRef]
28. Adem, E.; Burillo, G.; Dakin, V.; Vazquez, M. Promoting Polyethylene Foams by Irradiation Cross-Linking in Mexico. *Radiat. Phys. Chem.* **1995**, *46*, 937–940. [CrossRef]
29. Wang, B.; Wang, M.H.; Xing, Z.; Zeng, H.Y.; Wu, G.Z. Preparation of radiation crosslinked foams from low-density polyethylene/ethylene-vinyl acetate (LDPE/EVA) copolymer blend with a supercritical carbon dioxide approach. *J. Appl. Polym. Sci.* **2013**, *127*, 912–918. [CrossRef]
30. Auhl, D.; Stange, J.; Münstedt, H.; Krause, B.; Voigt, D.; Lederer, A.; Lappan, U.; Lunkwitz, K. Long-Chain Branched Polypropylenes by Electron Beam Irradiation and Their Rheological Properties. *Macromolecules* **2004**, *37*, 9465–9472. [CrossRef]
31. Findley, W.N.; Lai, J.S.; Onaran, K. *Creep and Relaxation of Nonlinear Viscoelastic Materials: With an Introduction to Linear Viscoelasticity*; Dover Publications, Inc.: New York, NY, USA, 1989.
32. Paggi, M.; Sapora, A. An Accurate Thermoviscoelastic Rheological Model for Ethylene Vinyl Acetate Based on Fractional Calculus. *Int. J. Photoenergy* **2015**, *2015*, 252740. [CrossRef]
33. Sharma, P.; Munro, P.A.; Gillies, G.; Wiles, P.G.; Dessev, T.T. Changes in creep behavior and microstructure of model Mozzarella cheese during working. *Lwt-Food Sci. Technol.* **2017**, *83*, 184–192. [CrossRef]
34. Hao, A.; Chen, Y.; Chen, J. Creep and Recovery Behavior of Kenaf/Polypropylene Nonwoven Composites. *J. Appl. Polym. Sci.* **2014**, *131*, 40726–40737. [CrossRef]
35. Ghannam, M.T. Creep–recovery experimental investigation of crude oil–polymer emulsions. *J. Appl. Polym. Sci.* **2004**, *92*, 226–237. [CrossRef]
36. Bayarri, S.; Dolz, M.; Hernández, M.J. Effect of carboxymethyl cellulose concentration on rheological behavior of milk and aqueous systems. A creep and recovery study. *Appl. Polym. Sci.* **2009**, *114*, 1626–1632. [CrossRef]
37. Villarreal, M.E.; Iturriaga, L.B. Viscoelastic properties of amaranth starch gels and pastes. Creep compliance modeling with Maxwell model. *Starch-Starke* **2016**, *68*, 1073–1083. [CrossRef]
38. Durmuş, A.; Woo, M.; Kaşgöz, A.; Macosko, C.W.; Tsapatsis, M. Intercalated linear low density polyethylene (LLDPE)/clay nanocomposites prepared with oxidized polyethylene as a new type compatibilizer: Structural, mechanical and barrier properties. *Eur. Polym. J.* **2007**, *43*, 3737–3749. [CrossRef]
39. Mussatti, F.G.; Macosko, C.W. Rheology of network forming systems. *Polym. Eng. Sci.* **1973**, *13*, 236–240. [CrossRef]
40. Chiu, F.C.; Fu, Q.; Hsieh, E.T. Molecular weight dependence of melt crystallization behavior and crystal morphology of low molecular weight linear polyethylene fractions. *J. Polym. Res.* **1999**, *6*, 219–229. [CrossRef]
41. Nicholson, L.M.; Whitley, K.S.; Gates, T.S. The role of molecular weight and temperature on the elastic and viscoelastic properties of a glassy thermoplastic polyimide. *Int. J. Fatigue* **2002**, *24*, 185–195. [CrossRef]
42. Dutta, J.; Ramachandran, P.; Ismail, S.M.R.S.; Naskar, K. Melt Rheological Behavior and Creep Response of EVA/TPU Blends: Exploring the Effect of Electron Beam Irradiation and Peroxide Cross-linking. *Polym.-Plast. Technol. Eng.* **2017**, *56*, 421–434. [CrossRef]
43. Svoboda, P. High-temperature study of radiation cross-linked ethylene-octene copolymers. *Polym. Bull.* **2017**, *74*, 121–144. [CrossRef]
44. Roscoe, R. Mechanical Models for the Representation of Visco-Elastic Properties. *Br. J. Appl. Phys.* **1950**, *1*, 171. [CrossRef]
45. McNally, T.; Pötschke, P.; Halley, P.; Murphy, M.; Martin, D.; Bell, S.E.J.; Brennan, G.P.; Bein, D.; Lemoine, P.; Quinn, J.P. Polyethylene multiwalled carbon nanotube composites. *Polymer* **2005**, *46*, 8222–8232. [CrossRef]
46. Datta, S.; Naskar, K.; Bhardwaj, Y.; Sabharwal, S. A study on dynamic rheological characterisation of electron beam crosslinked high vinyl styrene butadiene styrene block copolymer. *Polym. Bull.* **2011**, *66*, 637–647. [CrossRef]
47. Shin, B.Y.; Ha, M.H.; Han, D.H. Morphological, Rheological, and Mechanical Properties of Polyamide 6/Polypropylene Blends Compatibilized by Electron-Beam Irradiation in the Presence of a Reactive Agent. *Materials* **2016**, *9*, 342. [CrossRef]
48. Bai, L.; He, S.Y.; Fruehwirth, J.W.; Stein, A.; Macosko, C.W.; Cheng, X. Localizing graphene at the interface of cocontinuous polymer blends: Morphology, rheology, and conductivity of cocontinuous conductive polymer composites. *J. Rheol.* **2017**, *61*, 575–587. [CrossRef]
49. Kraft, M.; Meissner, J.; Kaschta, J. Linear viscoelastic characterization of polymer melts with long relaxation times. *Macromolecules* **1999**, *32*, 751–757. [CrossRef]

50. López-Barrón, C.R.; Macosko, C.W. Rheological and morphological study of cocontinuous polymer blends during coarsening. *J. Rheol.* **2012**, *56*, 1315–1334. [CrossRef]
51. Ramarad, S.; Ratnam, C.T.; Khalid, M.; Chuah, A.L. Improving the properties of reclaimed waste tire rubber by blending with poly(ethylene-co-vinyl acetate) and electron beam irradiation. *J. Appl. Polym. Sci.* **2015**, *132*, 41649–41657. [CrossRef]
52. Wang, B.B.; Hong, N.N.; Shi, Y.Q.; Wang, B.; Sheng, H.B.; Song, L.; Tang, Q.B.; Hu, Y. Comparative study on the effect of electron beam irradiation on the physical properties of ethylene-vinyl acetate copolymer composites. *Radiat. Phys. Chem.* **2014**, *97*, 284–291. [CrossRef]
53. Munusamy, Y.; Ismail, H.; Mariatti, M.; Ratnam, C.T. Effect of Electron Beam Irradiation on the Properties of Ethylene-(vinyl acetate) Copolymer/Natural Rubber/Organoclay Nanocomposites. *J. Vinyl Addit. Technol.* **2009**, *15*, 39–46. [CrossRef]
54. Michael, F.M.; Khalid, M.; Ratnam, C.T.; Walvekar, R.; Ramarad, S.; Ramli, S. Effect of electron beam irradiation on (waste tire dust)-filled ethylene vinyl acetate in the presence of bisphenol a diglycidyl ether. *J. Vinyl Addit. Technol.* **2017**, *23*, 172–180. [CrossRef]
55. Hwang, T.Y.; Lee, S.; Kang, P.H.; Park, K.H.; Ahn, Y.; Lee, J.W. The effect of electron beam irradiation on the dispersion and properties of poly(ethylene-co-vinyl acetate)/clay nanocomposites. *Macromol. Res.* **2011**, *19*, 1151–1156. [CrossRef]
56. Rezaeian, I.; Jafari, S.H.; Zahedi, P.; Ghaffari, M.; Afradian, S. Improvements of physical and mechanical properties of electron beam irradiation-crosslinked EVA foams. *Polym. Adv. Technol.* **2009**, *20*, 487–492. [CrossRef]
57. Gad, Y.H. Improving the properties of poly(ethylene-co-vinyl acetate)/clay composite by using electron beam irradiation. *Nucl. Instrum. Methods Phys. Res. Sect. B-Beam Interact. Mater. At.* **2009**, *267*, 3528–3534. [CrossRef]
58. Matsui, T.; Shimoda, M.; Osajima, Y. Mechanical Changes of Electron-Beam Irradiated Ethylene Vinyl-Acetate Copolymer (Eva) Film (1). *Polym. Int.* **1992**, *29*, 85–90. [CrossRef]
59. Hamid, Y.; Svoboda, P.; Svobodova, D. Influence of Electron Beam Irradiation on High-Temperature Mechanical Properties of Ethylene Vinyl Acetate/Carbon Fibers Composites. *J. Vinyl Addit. Technol.* **2020**, *26*, 325–335. [CrossRef]
60. Hui, J.; Xia, H.; Fu, Y.Q.; Qiu, Y.P.; Ni, Q.Q. Two-Way Reversible Shape Memory Properties of Benzoyl Peroxide Crosslinked Poly(ethylene-co-vinyl acetate) under Different Stress Conditions. *Macromol. Mater. Eng.* **2020**, *305*, 1900825. [CrossRef]
61. Qi, X.M.; Yang, W.T.; Yu, L.M.; Wang, W.J.; Lu, H.H.; Wu, Y.L.; Zhu, S.W.; Zhu, Y.F.; Liu, X.D.; Dong, Y.B.; et al. Design of Ethylene-Vinyl Acetate Copolymer Fiber with Two-Way Shape Memory Effect. *Polymers* **2019**, *11*, 1599. [CrossRef]